

1 **Theoretical study of mixing in liquid clouds.**

2 **Part 1: classical concept**

3

4 **Alexei Korolev<sup>1</sup>, Alex Khain<sup>2</sup>, Mark Pinsky<sup>2</sup>, and Jeffrey French<sup>3</sup>**

5 [1] Environment Canada, Cloud Physics and Severe Weather Section, Toronto, Canada

6 [2] Department of Atmospheric Sciences, the Hebrew University of Jerusalem, Israel

7 [3] University of Wyoming, Laramie, WY, USA

8 Correspondence to: A. Korolev ([alexei.korolev@canada.ca](mailto:alexei.korolev@canada.ca))

9

10

11

12 **Abstract**

13 The present study considers final stages of in-cloud mixing in the framework of classical  
14 concept of homogeneous and extreme inhomogeneous mixing. Simple analytical relationships  
15 between basic microphysical parameters were obtained for homogeneous and extreme  
16 inhomogeneous mixing based on the adiabatic consideration. It was demonstrated that during  
17 homogeneous mixing the functional relationships between the moments of the droplets size  
18 distribution hold only during primary stage of mixing. Subsequent random mixing between already  
19 mixed parcels and undiluted cloud parcels breaks these relationships. However, during extreme  
20 inhomogeneous mixing the functional relationships between the microphysical parameters hold  
21 both for primary and subsequent mixing. The obtained relationships can be used to identify the  
22 type of mixing from in situ observations. The effectiveness of the developed method was  
23 demonstrated using in-situ data collected in convective clouds. It was found that for the specific  
24 set of in-situ measurements the interaction between cloudy and entrained environments was  
25 dominated by extreme inhomogeneous mixing.

26

27

28

29

30

31

## 32 **1 Introduction**

33 Turbulent mixing is an important non-adiabatic process in the atmosphere that to a large extent  
34 determines spatial gradients of many thermodynamic (e.g. temperature, humidity) and cloud  
35 microphysical parameters (e.g. hydrometeor concentrations, extinction coefficient, condensed  
36 water content) and as such, needs to be properly described in numerical simulations of clouds and  
37 weather predictions. Entrainment and mixing occurs during the entire lifetime of a cloud and is  
38 active not only near cloud edges, but it is important throughout the whole cloud volume. Mixing  
39 of cloudy and entrained air results in changes to the shape of the droplet size distribution through  
40 partial droplet evaporation and can also lead to changes in droplet concentration through complete  
41 evaporation of some fraction of droplets and dilution. The shape of the droplet size distribution  
42 plays key role in the initiation of precipitation and radiative properties of clouds.

43 The treatment of mixing in numerical simulations of clouds and precipitation formation  
44 remains a challenging problem. Besides the issues related to the way to describe mixing in  
45 numerical schemes, there is a fundamental problem of identifying a scenario or path, that mixing  
46 events should follow. Through the pioneering works of Latham and Reed (1977) and Baker et al.  
47 (1980) two explicitly alternative scenarios of mixing were identified. In the first scenario turbulent  
48 mixing rapidly stirs the environment homogenizing the fields of temperature and humidity.  
49 Following that, all of the droplets undergo partial evaporation under the same conditions. The result  
50 of this mixing is a droplet population with reduced sizes, but a total number that remains  
51 unchanged. This type of mixing is referred to as *homogeneous*. In the second scenario mixing  
52 occurs more slowly such that the population of droplets experiences different amount of sub-  
53 saturation. Some number of droplets completely evaporates, while others experience no  
54 evaporation until the entirety of the entrained air becomes saturated. Following that, turbulence  
55 mixes the rest of the droplets with the saturated, but droplet-free environment. During this type of  
56 mixing the size of droplets remains unchanged; however, their total number is reduced. This type  
57 of mixing is called *extreme inhomogeneous*. The intermediate case when some fraction of droplets  
58 evaporates partially, another other fraction evaporates completely, and a third fraction remains  
59 unchanged is in some works referred to as inhomogeneous (e.g. Baker and Latham, 1980).

60 The conditions for homogeneous and extreme inhomogeneous mixing and their effects on  
61 precipitation formation have been debated in cloud physics over forty years. There are a number  
62 of numerical simulations and theoretical efforts on studying different aspects of mixing and its

63 effect on cloud microphysics (e.g. Baker and Latham, 1982; Jensen and Baker, 1989; Su et al.,  
64 1989; Lasher-Trapp et al., 2005; Jeffrey, 2007; Andrejczuk et al., 2009; Kumar et al., 2013; Jarecka  
65 et al. 2013 and many others). A comprehensive review of the works on the effect of turbulence and  
66 mixing on cloud droplet formation can be found in Devenish et al. (2012).

67 A number of studies were dedicated to identifying type of mixing based on in-situ  
68 observations. Most of the previous observations provided evidence supporting inhomogeneous  
69 mixing (e.g. Hill and Choulaton, 1985; Paluch, 1986; Bower and Choulaton, 1988; Blyth and  
70 Latham, 1991; Gerber et al., 2008, Lu et al. 2011; Beals et al. 2016). However, works of Jensen  
71 and Baker (1989), Paluch and Baumgardner (1989), Burnet and Brenguier (2007), Lehmann et al.  
72 (2009), Lu et al. (2011) suggested occurrence of homogeneous mixing. So, at the moment it appears  
73 that both types of mixing may occur in liquid clouds. However, the environmental conditions  
74 governing one or the other type of mixing remain not well understood.

75 Early experimental work on identifying type of mixing from in-situ observations were based  
76 on the analysis of spatial variability of the shapes of individual droplet size distributions (e.g.  
77 Paluch and Knight, 1984; Paluch, 1986; Bower and Choulaton, 1988). The effectiveness of this  
78 method involving the analysis of a large number of individual size spectra turned out to be quite  
79 low. Another technique utilized expected functional relationships between droplet concentration  
80 ( $N$ ) and droplet diameter ( $D$ ) specific to each type of mixing. Thus, during extreme inhomogeneous  
81 mixing the droplet size is expected to remain unchanged, whereas the concentration will vary.  
82 During homogeneous mixing the droplet size and concentration in cloud will be related to each  
83 other in a certain way, depending on the mixing fraction and the humidity of the entrained air. This  
84 fact was used in observational studies for identifying the type of mixing from “mixing diagrams”  
85 that related  $N$  and  $D_v$  for different regimes of mixing (e.g. Burnet and Brenguier, 2007; Gerber et  
86 al., 2008; Lehmann et al., 2009).

87 The use of mixing diagrams to some extent facilitated identification of type of mixing.  
88 However, in many cases scatter in the relationships between  $N$  vs.  $D_v$  was too large, hindering  
89 identification of the type of mixing (Burnet and Brenguier, 2007). To resolve this problem many  
90 researchers used other complementary measurements supporting identification of the type of  
91 mixing (e.g. Gerber et al., 2008; Lehmann et al., 2009).

92 Besides the effect on  $N$  and  $D_v$ , the type of mixing is anticipated to manifest itself in  
93 relationships between other moments of the droplet size distribution,  $f(D)$ . Such relationships may

94 provide insight into the mixing process and identify type of mixing. With the exception of the work  
95 by Hill and Choulaton (1985), who correlated concentration and liquid water content, there have  
96 been few attempts to use any other microphysical parameters for identification of type of mixing.

97 In order to fill this gap, this study presents a theoretical analysis of relationships between  
98 different moments of  $f(D)$  within the framework of homogeneous and extreme inhomogeneous  
99 mixing. The analysis is focused on the first four moments of  $f(D)$  corresponding to the droplet  
100 concentration  $N$  (0<sup>th</sup> moment), integral diameter  $N\bar{D}$  (1<sup>st</sup> moment), extinction coefficient  $\beta$  (2<sup>nd</sup>  
101 moment), liquid water mixing ratio  $q$  (3<sup>rd</sup> moment) and mean volume diameter  $D_v$  (mixed 3<sup>rd</sup> and  
102 0<sup>th</sup> moment). It is shown that the newly obtained relationships between the moments provide a  
103 more robust identification of type of mixing from in-situ measurements as compared to  
104 conventional  $N - D_v^3$  relationships used in mixing diagrams. Relationships between moments may  
105 be useful for parameterization of mixing in numerical simulations of clouds and climate,  
106 interpretations of remote sensing measurements.

107 This paper constitutes the first in a series of three papers. It considers the final stage of  
108 mixing based on the formal definitions of homogeneous and extreme inhomogeneous mixing.  
109 These two types of mixing present two extreme regimes of mixing. The following two papers  
110 provide a detailed analysis of the time dependent processes during homogeneous (Pinsky et al.,  
111 2016a) and inhomogeneous (Pinsky et al., 2016b) mixing where non-extreme regimes are  
112 considered as well.

113 This paper is arranged in the following way. Section 2 presents analysis of the analytical  
114 relationship between  $N$ ,  $N\bar{D}$ ,  $\beta$ ,  $q$ ,  $D_v$  and mixing fraction  $\mu$  for the cases of homogeneous and  
115 extreme inhomogeneous mixing. In Sect. 3 the obtained analytical relationships are compared with  
116 the results of numerical simulation of  $N$ ,  $\beta$ ,  $q$ ,  $D_v$  formed at the final stage of mixing. Section 4  
117 presents results of simulation of progressive mixing and it effect of the relationships between  
118 moments. Examples of relationship between  $N$ ,  $\beta$ ,  $q$  and  $D_v$  from in-situ observations are  
119 presented in Sect. 5. The discussion and concluding remarks are presented in Sect. 6 and 7.

120

## 121 **2 Effect of mixing on microphysical variables**

### 122 **2.1 Phenomenological consideration**

123 The conceptual diagrams of homogeneous and extreme inhomogeneous mixing are shown on  
124 Fig. 1. During the first stage of extreme inhomogeneous mixing the subsaturated parcel is engulfed

125 into the cloudy environment (Fig. 1a1). Then, the droplets at the interface of the sub-saturated  
126 parcel and the cloud environment undergo complete evaporation until the air within the engulfed  
127 volume reaches saturation (Fig. 1a2). After that the saturated but droplet free parcel mixes with the  
128 rest of the cloud environment (Fig. 1a3). The result of inhomogeneous mixing is that the cloud  
129 parcel has reduced droplet concentration and the droplet sizes remain unchanged.

130 In the case of homogeneous mixing after entraining into a cloud (Fig. 1b1), the subsaturated  
131 parcel “instantly” mixes up with its cloud environment (Fig. 1b2) leading to undersaturation of the  
132 total volume. Then, all droplets throughout the mixed volume undergo simultaneous evaporation  
133 until the equilibrium state is reached. The result of homogeneous mixing is a cloud volume with  
134 reduced concentration of droplets and droplets with reduced sizes (Fig. 1b3).

135 Based on mass and energy conservation considerations the final state of the bulk parameters  
136 (i.e. liquid water mixing fraction, humidity, temperature, etc.) is the same for both types of mixing.  
137 However, in the case of extreme inhomogeneous mixing saturation is reached through complete  
138 evaporation of some fraction of droplets, and their sizes remain constant. Whereas in case of  
139 homogeneous mixing saturation is reached through a uniform evaporation of droplets, and the total  
140 number of droplets remains unchanged. It should be noted, that in both cases the droplet  
141 concentration decreases due to dilution by the mixed droplet free sub-saturated parcel.

142 The following discussion will be specifically focused on the microphysical properties formed  
143 at the final stage of the homogeneous and extreme inhomogeneous mixing. The processes occurring  
144 during mixing state (i.e. transition 1a→2a and 1b→2b in Fig. 1) remain outside the frame of this  
145 work. Following the formalism of homogeneous and extreme inhomogeneous mixing, the process  
146 of mixing reaches the final stage when (1) the entrained and cloud environment are mixed up and  
147 the spatial gradients of the microphysical ( $N$ ,  $\beta$ ,  $q$ , etc.) and environmental ( $T$ ,  $S$ ,  $e$ , etc.) parameters  
148 approach to zero; (2) the diffusional process related to droplet evaporation comes into equilibrium.  
149 The second condition is completed when (a) the environment reaches saturation state, or (b) the  
150 entire population of droplets is completely evaporated, if the entrained air is sufficiently dry.

151 The above description of homogeneous and extreme inhomogeneous mixing is highly  
152 idealized. Actual in-cloud mixing does not occur as a sequence of discrete events (Fig.1) that  
153 individually come to equilibrium only to be followed by next discrete mixing events. But rather it  
154 is occurring continuously on a cascade of different spatial and time scales. Broadwell and  
155 Breidenthal (1982) summarized the experimental evidence and proposed the following description

156 of mixing in turbulent shear layers. Mixing takes place in a series of events. Two shear layers  
157 exchange mass by engulfing parcels from an opposite layer into localized zones. The initially large-  
158 scale filaments of the two gases break down towards smaller scales due to the action of turbulence.  
159 The turbulence stretches the interface between the gases and enhances the molecular diffusion  
160 across the increasing surface. The actual mixing of the engulfed volume is a molecular diffusion  
161 process that is most effective after the break down volumes reduce to the Kolmogorov viscosity  
162 scale. It is anticipated that the reaction of the ensemble of droplets is a combination of  
163 homogeneous and inhomogeneous mixing with domination of one type of mixing over the other  
164 depending on the characteristic spatial and time scales of the environment determined by  
165 turbulence, cloud microphysics, state parameters and stage of mixing.

166

## 167 **2.2 Methodology**

168 The foregoing discussion will be focused on mixing between saturated cloud parcels and out-  
169 of-cloud sub-saturated air. The cloud parcel contains droplets with average diameter  $\bar{D}_1$ , liquid  
170 mixing ratio  $q_1$  and number concentration  $N_1$ . The initial temperature in the cloud parcel is  $T_1$ ,  
171 relative humidity  $RH_1 = 1$ , where  $RH = e/e_s(T)$  (the explanation of variable notations is provided  
172 in Table 1). The second parcel is droplet free ( $N_2 = 0$ ), sub-saturated with initial relative humidity  
173  $RH_2 < 1$  and temperature  $T_2$ . The mixing occurs isobarically, i.e.  $p = \text{const}$ . At the final stage of  
174 mixing the temperature and humidity formed in the resulting parcel are  $T$  and  $RH$  (appendix A).  
175 The process of mixing is completed when the mixed parcel reaches equilibrium due to the air  
176 saturation (i.e.  $RH = 1$ ), or due to the complete evaporation of droplets. In the latter case the final  
177 humidity is  $RH \leq 1$ . The effect of the vertical velocity and vertical travel on final  $T$ ,  $RH$ , and  $q$  is  
178 not considered here, i.e. vertical velocity  $u_z = 0$ .

179 Without the loss of generality the masses of the cloudy and sub-saturated volumes prior to the  
180 mixing are assumed to have a unit masses, i.e.  $m_1 = 1$  and  $m_2 = 1$ . The mixing process will be  
181 considered as mixing of  $\mu$  fraction of the cloud parcel with  $(1 - \mu)$  fraction of the second (sub-  
182 saturated) parcel. The mixing cloud fraction may vary within the range of  $0 \leq \mu \leq 1$ . Therefore,  
183 the mass of the resulting mixed parcel is equal to  $m_1\mu + (1 - \mu)m_2 = 1$ . This approach simplifies  
184 the consideration of mixing and allows considering all possible proportions of the mixing of two  
185 volumes.

186

### 2.3 Effect of mixing on liquid water and temperature

The mixing ratio of liquid water  $q$  formed at the final stage of mixing is determined by the mass of the mixing cloud water  $\mu q_1$  and amount of evaporated water required to saturate the newly formed mixed volume  $\delta q_m$ . The mass balance of liquid water for the mixing volume yields

$$q = \mu q_1 - \delta q_m, \quad (1)$$

where

$$\delta q_m = \frac{c_p R_v T_{m0}^2}{L^2} \ln \left( \frac{1 + \frac{e_s(T_{m0}) R_a L^2}{p c_{pa} R_v^2 T_{m0}^2}}{1 + RH_{m0} \frac{e_s(T_{m0}) R_a L^2}{p c_{pa} R_v^2 T_{m0}^2}} \right) \cong -\frac{S_{m0}}{A_2} \quad (2)$$

is the mixing ratio of liquid water required to saturate 1kg of volume with temperature  $T_{m0}$  and humidity  $RH_{m0}$  (appendix A);  $T_{m0}$ ,  $RH_{m0}$  and  $S_{m0}$ , are the temperature, relative humidity formed and supersaturation formed in the volume after instantaneous air mixing, but before droplets start evaporating (appendix A);  $e_s(T_{m0})$  is saturation vapor pressure at temperature  $T_{m0}$ .

Eq. (1) is a non-linear function of  $\mu$ , since  $T_{m0}$ ,  $e_{m0}$  and thus  $\delta q_m$  depend on  $\mu$ . Eq.(1) can be simplified, if  $T_1 = T_2$ . In this case  $T_{m0} = T_1 = T_2$ , and  $e_s(T_{m0}) = e_s(T_1) = e_s(T_2)$ . Given that, the expression under logarithm in Eq.(2) can be expanded in series resulting in (appendix B)

$$\delta q_m = (1 - \mu) \delta q^*, \quad (3)$$

where

$$\delta q^* = \frac{c_p R_v T_2^2}{L^2} \ln \left( \frac{1 + \frac{e_s(T_2) R_a L^2}{p c_{pa} R_v^2 T_2^2}}{1 + RH_2 \frac{e_s(T_2) R_a L^2}{p c_{pa} R_v^2 T_2^2}} \right) \cong -\frac{S_2}{A_2} \quad (4)$$

is the mixing ratio of liquid water required to saturate 1 kg of the entrained dry air. Substituting Eq.(3) in Eq.(1) gives

$$q = \mu q_1 - (1 - \mu) \delta q^*, \quad (5)$$

The value of  $\delta q^*$  does not depend on  $\mu$ , and Eq. (5) is a simple linear function of  $\mu$ . The comparisons with numerical simulations showed, that Eq.(5) provides accuracy within few percent, when the temperature difference  $|T_1 - T_2| < 2^\circ\text{C}$ . Although, in many cases  $|T_1 - T_2|$  may vary a

210 wide range reaching 10°C or higher, clouds with  $|T_1 - T_2| < 2^\circ\text{C}$  are quite common. Therefore, for  
 211 the sake of simplicity, Eq.(5) and the assumption  $T_1 \approx T_2$  will be used in the following  
 212 consideration of mixing.

213 It should be noted that, Eqs (1) and (5) are valid for the cases, when  $\mu > \mu_{cr}$ . Here  $\mu_{cr}$  is  
 214 critical mixing fraction, which separates partial and complete evaporation of cloud water in the  
 215 mixing volume (section 2.4). Cases when  $\mu \leq \mu_{cr}$  correspond to complete evaporation of droplets,  
 216 and  $q = 0$ .

217 The temperature at the final stage of mixing can be estimated as (appendix C)

$$218 \quad T = T_{m0} - \frac{(1 - \mu)\delta q^* L}{c_{pa}}, \quad \text{when } \mu > \mu_{cr} \quad (6a)$$

$$219 \quad T = T_{m0} - \frac{\mu q_1 L}{c_{pa}} \quad \text{when } \mu \leq \mu_{cr} \quad (6b)$$

220 Eqs. (1), (5), (6) were obtained based on mass and energy conservation, and they do not depend  
 221 on how mixing proceeds. Therefore, Eqs. (1), (5), (6) are valid for both homogeneous and  
 222 inhomogeneous mixing.

223

## 224 **2.4 Complete evaporation**

225 As mentioned in section 2.2 the process of mixing is complete only after reaching equilibrium  
 226 by saturating the mixed volume or by evaporating of all cloud droplets depending on the mixing  
 227 fraction  $\mu$ . The critical mixing fraction  $\mu_{cr}$ , corresponding to evaporation of all droplets, can be  
 228 found from Eq.(5) when  $q = 0$ , i.e.

$$229 \quad \mu_{cr} = \frac{\delta q^*}{q_1 + \delta q^*} \quad (7)$$

230 Critical mixing fraction separates  $\mu$  in two subranges: (a)  $1 \geq \mu > \mu_{cr}$  where  $q$  is described  
 231 by Eqs.(1) or (5) and  $RH_m = 1$ ; (b)  $\mu_{cr} \geq \mu \geq 0$  where  $q = 0$  and  $RH_m \leq 1$ .

232 For the general case when  $T_1 \neq T_2$ ,  $\mu_{cr}$ , can be found by solving the non-linear equation

$$233 \quad \mu_{cr} q_1 - \delta q_m(\mu_{cr}) = 0 \quad (8)$$

234 Figure 2 shows comparisons of dependences of  $\mu_{cr}$  vs.  $q_1$  calculated from Eq. (7) and those  
 235 deduced from a numerical model (Sect. 3). Critical mixing fraction  $\mu_{cr}$  is also shown by black stars  
 236 in Fig. 4. The locations of the stars in Fig.4 coincide well with the locations, where the modeled



237 microphysical moments become zero. The obtained agreement between analytical and modeled  
 238  $\mu_{cr}$  in Figs. 2 and 4 validates the developed approach.

239

## 240 **2.5 Extreme inhomogeneous mixing**

241 Within the framework of extreme inhomogeneous mixing some fraction of droplets undergo  
 242 complete evaporation, whereas the rest of the droplets remain unchanged. Therefore, such a process  
 243 results in scaling the droplet size distribution  $f(D)$ , i.e.

$$244 \quad f(D) = kf_1(D) \quad (9)$$

245 where  $k$  is some coefficient dependent on  $\mu$  and the initial environmental parameters of the mixing  
 246 volumes,  $f_1(D)$  is the droplet size distribution before mixing. Equation (9) yields relationships  
 247 between pairs  $n$ th and  $k$ -th moments

$$248 \quad \frac{M_n}{M_{n1}} = \frac{M_k}{M_{k1}} \quad (10)$$

249 where  $M_n = \int_0^{\infty} f(D)D^n dD / \int_0^{\infty} f(D)dD$  is the  $n$ th moment of  $f(D)$ . Therefore, it is anticipated that

250 for extreme inhomogeneous mixing droplet number concentration  $N$  (0th moment), extinction  
 251 coefficient  $\beta$  (2nd moment), liquid water mixing ratio  $q$  (3rd moment), along with other moments,  
 252 will correlate with each other, i.e.

$$253 \quad \frac{N}{N_1} = \frac{\beta}{\beta_1} = \frac{q}{q_1} \quad (11)$$

254 One of the consequences of Eqs. (9)-(11) is that the characteristic droplet sizes  $\bar{D}$ ,  $D_2$ ,  $D_v$ ,  $D_{eff}$   
 255 will remain constant during inhomogeneous mixing.

256 For the case  $T_1 = T_2$  and  $\mu > \mu_{cr}$  Eqs. (5) and (11) yield the dependence of  $N$  vs.  $\mu$

$$257 \quad N = N_1 \left( \mu - \frac{(1-\mu)\delta q^*}{q_1} \right) \quad (12)$$

$$258 \quad \beta = \beta_1 \left( \mu - \frac{(1-\mu)\delta q^*}{q_1} \right) \quad (13)$$

259 For a general case when  $T_1 \neq T_2$  the term  $(1-\mu)\delta q^*$  in Eqs. (12) and (13) should be replaced  
 260 by  $\delta q_m(\mu)$  (Eq.(2)).

261

262 **2.6 Homogeneous mixing**

263 For homogeneous mixing, when  $\mu > \mu_{cr}$ , the droplet number concentration changes only due  
 264 to dilution by the entrained air, i.e.

$$265 \quad \frac{N}{N_1} = \mu \quad (14)$$

266 Assuming  $T_1 = T_2$ , and substituting Eq. (5) in (14) yields:

$$267 \quad \frac{N}{N_1} = \frac{q + \delta q^*}{q_1 + \delta q^*} \quad (15)$$

268 As follows from Eq. (15)  $N$  and  $q$  are linearly related for homogeneous mixing. However, no  
 269 linear relationships exist between other moments. Thus, substituting the definition of the liquid  
 270 water mixing ratio  $q = \pi \rho_w N D_v^3 / 6 \rho_a$  in Eq. (15) yields the relationship between mean volume  
 271 droplet size and concentration

$$272 \quad \frac{D_v^3}{D_{v1}^3} = 1 + \left(1 - \frac{N_0}{N}\right) \frac{\delta q^*}{q_1} \quad (16a)$$

$$273 \quad \frac{D_v^3}{D_{v1}^3} = \frac{q}{q_1} \left( \frac{q_1 + \delta q^*}{q + \delta q^*} \right) \quad (16b)$$

274 In a similar way the relationship between the extinction coefficient  $\beta = Q \pi N D_2^2 / 4$ ,  $N$  and  $q$   
 275 can be written as

$$276 \quad \frac{\beta}{\beta_1} = \frac{N}{N_1} \left( 1 + \left(1 - \frac{N_0}{N}\right) \frac{\delta q^*}{q_1} \right)^{2/3} \quad (17a)$$

$$277 \quad \frac{\beta}{\beta_1} = \left( \frac{q}{q_1} \right)^{2/3} \left( \frac{q + \delta q^*}{q_1 + \delta q^*} \right)^{1/3} \quad (17b)$$

278 In Eqs. (17a) and (17b) it is assumed that  $D_2 \approx D_v$ .

279 Substituting in Eq. (16) the expression for the time of phase relaxation  
 280  $\tau_p = 1/bN\bar{D}$  (e.g. Squires 1953; Korolev and Mazin, 2003) and assuming  $\bar{D} \approx D_v$  yields

$$281 \quad \frac{\tau}{\tau_1} = \frac{N_1}{N} \left( 1 + \left(1 - \frac{N_1}{N}\right) \frac{\delta q^*}{q_1} \right)^{-1/3} \quad (18)$$

282 For the cases when the temperature difference  $|T_1 - T_2|$  exceeds a few degrees, the effect of  $\mu$   
 283 on  $T_m$  and  $S_m$  should be taken into consideration in the calculations of evaporated water. For such

284 cases  $\delta q_m$  (Eq. (2)) should be used instead of  $\delta q^*$ . Using Eq. (14)  $\delta q_m$  can be presented as a  
 285 function of  $\frac{N}{N_1}$ , i.e.  $\delta q_m(\mu) = \delta q_m\left(\frac{N}{N_1}\right)$ . Replacing Eq. (5) by (1) in the above consideration, the  
 286 equations Eqs. (15)-(18) can be rewritten as

$$287 \quad \frac{N}{N_1} = \frac{q + \delta q_m\left(\frac{N}{N_1}\right)}{q_1} \quad (19)$$

$$288 \quad \frac{D_v^3}{D_{v1}^3} = 1 - \frac{\delta q_m\left(\frac{N}{N_1}\right) \frac{N_1}{N}}{q_1} = \frac{q}{q + \delta q_m\left(\frac{q}{q_1}\right)} \quad (20)$$

$$289 \quad \frac{\beta}{\beta_1} = \frac{N}{N_1} \left( 1 - \frac{\delta q_m\left(\frac{N}{N_1}\right) \frac{N}{N_1}}{q_1} \right)^{2/3} = \frac{q^{2/3} \left( q + \delta q_m\left(\frac{\beta}{\beta_1}\right) \right)^{1/3}}{q_1} \quad (21)$$

$$290 \quad \frac{\tau_p}{\tau_{p1}} = \frac{N_1}{N} \left( 1 - \frac{\delta q_m\left(\frac{N}{N_0}\right) \frac{N_1}{N}}{q_1} \right)^{-1/3} \quad (22)$$

291 Eqs. (19)–(22) can be solved numerically.

292

## 293 **2.7 Degenerate case**

294 As follows from Eq.(5), if

$$295 \quad \frac{(1-\mu)}{\mu} \frac{\delta q^*}{q_1} \ll 1 \quad (23)$$

296 then  $q_1 \geq q \gg \delta q^*$ . If the condition in Eq. (23) is valid, then the terms associated with  $\delta q^*$  in Eqs.  
 297 (15)-(18) can be neglected. This results in correlation of all moments, i.e.  $N/N_1 = \beta/\beta_1 = q/q_1$   
 298 (compare with Eq.(11)). This corresponds to the degenerate case, when the difference between the  
 299 homogeneous and inhomogeneous mixing vanishes. Thus, the dimensionless parameter  $\xi =$

300  $\frac{1-\mu}{\mu} \frac{\delta q^*}{q_1}$  can be used for characterization of proximity of the homogeneous mixing moments to those

301 formed during extremely inhomogeneous mixing.

302 The range of  $\mu$  in  $\xi$  is limited by  $\mu_{cr} < \mu \leq 1$ , so that  $0 < \frac{1-\mu}{\mu} \leq \frac{q_1}{\delta q^*}$ . This gives the range of  
 303 changes of  $\xi$ , i.e.  $0 \leq \xi \leq 1$  for the mixing without complete evaporation of droplets. The  
 304 degenerate case corresponds to  $\xi \rightarrow 0$ , whereas  $\xi \rightarrow 1$  corresponds to maximum difference of the  
 305 moments for homogeneous and extremely inhomogeneous mixing.

306 As follows from Eqs. (4) and (23) approaching to the degenerate case ( $\xi \rightarrow 0$ ) occurs, when  
 307 one of the following conditions or their combination is satisfied: (a)  $RH_2 \rightarrow 1$ ; (b)  $E_s(T) \rightarrow 0$  at  
 308 low temperatures; (c)  $q_1 \gg \delta q^*$ ; (d)  $\mu \rightarrow 1$ . The effect of  $RH$ ,  $T$ ,  $q_1$  and  $\mu$  on mixing will be  
 309 demonstrated in Sect.3.

310 Figure 3 shows dependence of  $\xi$  vs.  $\mu$ . The grey area in Fig.3 indicates the region where  
 311 identification of type of mixing from in-situ measurements (Sect.5) may be hindered due to  
 312 proximity of the moments for homogeneous and inhomogeneous mixing. Thus for  $\delta q^*/q_1 = 0.01$   
 313 identification of type of mixing is ambiguous for nearly the entire range of  $\mu$ .

314 For the general case, when  $T_1 \neq T_2$ , it should be  $\xi = \frac{|\delta q_m(\mu)|}{\mu q_1}$ . An absolute value  $|\delta q_m(\mu)|$   
 315 should be used in  $\xi$  since  $\delta q_m(\mu)$  can be negative (Appendix A, Fig.A1) if mixing results in  
 316 supersaturation Sect. 3.4).

317 The coefficient  $\xi$  may be useful for identification type of mixing from in-situ observations. It  
 318 is worth nothing, that the ratio  $\frac{\delta q^*}{q_1} \cong \frac{S_2}{A_2 q_1}$  is equal to the parameter  $R$  (Pinsky et al. 2015ab), which  
 319 plays an important role in determining scenarios of droplet evaporation in turbulent environment.

320

### 321 **3 Comparisons with numerical simulations**

322 Numerical simulations of the final stages of mixing were performed in order to examine the  
 323 accuracy and limitations of the analytical expressions obtained in the previous section. The  
 324 simulations have been conducted with the help of a parcel model similar to that described in  
 325 Korolev (1995). The ensemble of droplets in the simulation was assumed to be monodisperse. For  
 326 the case of extreme inhomogeneous mixing the amount of evaporated water  $\Delta q$  required to saturate  
 327 the mixed volume was calculated first. If  $\Delta q < \mu q_1$ , then the concentration of evaporated droplets  
 328 was calculated as  $N_{ev} = \frac{\Delta q}{m_d} \rho_a$ , where  $m_d = \pi \rho_w D^3 / 6$ . Then, the concentration of the remaining  
 329 droplets  $N = N_1 - N_{ev}$  was recalculated based of the calculation on the volume formed after  
 330 mixing. If  $\Delta q \geq \mu q_1$ , then all droplets evaporate, and  $N = 0$ .

331 For the case of homogeneous mixing in the first step the engulfed parcel instantly mixes with  
332 the cloud parcel resulting in a new humidity  $RH_{m0}$ , temperature  $T_{m0}$  and volume  $V_{m0}$ . After that  
333 the droplets start evaporating until either their complete evaporation or saturation over liquid is  
334 reached. The calculations stopped when, either  $D < 0.2\mu\text{m}$  or  $(E_S - e)/E_S < 0.001$ , respectively.

335

### 336 **3.1 Effect of mixing fraction**

337 Figure 4 shows the results of the simulation of different moments and state parameters vs.  $\mu$ .  
338 The calculations were performed for different relative humidity of the entrained parcel  $RH_2 = 0.2$ ,  
339 0.5, 0.8 and 0.95. As seen from Fig.4 for the case of homogeneous mixing only  $N$  and  $q$  are linearly  
340 related with  $\mu$ , the rest of the variables have non-linear dependences on  $\mu$ . For the case of  
341 inhomogeneous mixing all  $f(D)$  moments and droplet sizes linearly depend on  $\mu$ . Note, for  $\mu \leq$   
342  $\mu_{cr}$  all moments are equal to zero.

343 Since the amount of the evaporated liquid water does not depend on the type of mixing, the  
344 dependences of  $q(\mu)$  are the same for both homogeneous and inhomogeneous mixing (Fig.4a). The  
345 type of mixing has the most pronounced effect on the droplet concentration (Fig.4b) and droplet  
346 sizes (Fig.4e).

347 Figure 4g shows the dependences  $RH_{m0}$  and  $RH$  vs.  $\mu$ , Here  $RH_{m0}$  is the relative humidity at  
348 the initial stage of homogeneous mixing before droplets start evaporating (Fig. 1b2). Figure 3h  
349 presents comparisons of modeled  $T(\mu)$  and those calculated from Eqs.(6a,b) and (C4). The  
350 independence of  $q(\mu)$ ,  $RH(\mu)$  and  $T(\mu)$  on type of mixing (Fig.4a,g,h) is the consequence of the  
351 mass and energy conservation, which are not contingent on type of mixing.

352

### 353 **3.2 Effect of humidity of entrained air**

354 The diagrams in Fig. 5a-c show the dependences of normalized  $\beta$ ,  $q$  and  $D_v$  vs.  $N/N_0$   
355 calculated from numerical simulations and analytical equations from Sect. 2. The calculations were  
356 performed for different humidity of the entrained air  $RH_2$ . As seen from Fig. 5a-c, the normalized  
357 dependences for homogeneous mixing  $q(N)$ ,  $\beta(N)$  and  $D_v(N)$  tend to approach the line of extreme  
358 inhomogeneous mixing when relative humidity  $RH_2$  approaches to 1. This is consistent with the  
359 degenerate case, when  $\xi \rightarrow 0$  (Sect.2.7). In this case droplets behave as a passive admixture, and  
360 they do not interact with the environment.

361

362 **3.3 Effect of liquid water mixing ratio**

363 Figure 5d-f demonstrate the sensitivity of  $q(N)$ ,  $\beta(N)$  and  $D_v(N)$  to liquid water mixing ratio  
364  $q_1$ . It is seen, that the increase of  $q_1$  results in  $q(N)$ ,  $\beta(N)$  and  $D_v(N)$  (calculated for homogeneous  
365 mixing) approaching towards  $q(N)$ ,  $\beta(N)$  and  $D_v(N)$  for the inhomogeneous mixing. In other  
366 words, the sensitivity of the microphysical parameters to the type of mixing increases with the  
367 decrease of  $q_1$ . From a practical viewpoint it means, that from in-situ observations the difference  
368 between homogeneous and inhomogeneous mixing is anticipated to be more pronounced for the  
369 cases with a relatively low liquid water mixing ratio (e.g.  $q_1 < 1\text{g/m}^3$ ). Such behaviour is consistent  
370 with the consideration in Sect. 2.7.

371

372 **3.4 Effect of temperature  $T_1 = T_2$**

373 Figure 5g-j shows the effect of temperature on the normalized  $q(N)$ ,  $\beta(N)$  and  $D_v(N)$  for  $T_1 =$   
374  $T_2$ . Figure 5g-j indicate that the difference between the moments becomes most pronounced at  
375 warm temperatures, whereas at cold temperatures (e.g.  $T = -30^\circ\text{C}$ ),  $q(N)$ ,  $\beta(N)$  and  $D_v(N)$  for  
376 homogeneous mixing are approaching those for the extreme inhomogeneous mixing limit.

377 Such behavior is explained by the fact that liquid water deficit  $\delta q_m$  decreases with decreasing  
378 temperature (appendix A, Fig. A1). At low temperatures ( $T = -30^\circ\text{C}$ ) the amount of evaporated  
379 water  $\delta q_m$  is so small, that homogeneous mixing with dry out-of-cloud air will have approximately  
380 the same effect as mixing with saturated air (i.e. degenerate case, Sect. 2.7).

381 Overall, as follows from Fig.5 the results the analytical predictions (Sect. 2) turned out to be  
382 in a good agreement with numerical simulations.

383

384 **3.5 Effect of temperature  $T_1 \neq T_2$**

385 Isobaric mixing of two nearly saturated volumes with  $T_1 \neq T_2$  may result in supersaturated  
386 environment (e.g. Rogers, 1976; Bohren and Albrecht, 1998). Mixing resulting in supersaturation  
387 is different in principle from the mixing with evaporating droplets. In this case the meaning of  
388 homogeneous and inhomogeneous mixing becomes ambiguous. Formation of supersaturation leads  
389 to different dependences between  $N\bar{D}$ ,  $\beta$ ,  $q$ ,  $\bar{D}$  and  $N$  as compared to those shown in Figs. 3–4,  
390 when  $T_1 = T_2$ .

391 Figure 6 presents a set of diagrams similar to those in Fig.4, but calculated for the cases when  
392  $T_1 \leq T_2$ . It turns out that for the case of extreme inhomogeneous mixing the temperature difference

393 between  $T_1$  and  $T_2$  breaks down linear dependences of the microphysical moments (e.g.  $N\bar{D}$ ,  $\beta$ ,  $q$   
394 Fig. 6a,c,d) vs.  $\mu$ .

395 Figure 7 presents the effect of the temperature difference  $\Delta T$  on the normalized dependences  
396  $q(N)$ ,  $\beta(N)$  and  $D_v(N)$ . In clouds, high supersaturation resulting from isobaric mixing may lead  
397 to activation of interstitial CCN, which may increase  $N$  and decrease  $D_v$  (Korolev and Isaac, 2000).  
398 However, no activation of new droplets during isobaric mixing was allowed in this study. For the  
399 cases when  $RH_{m0} > 1$  (Fig. 7, AB on line 1) the condensed water was uniformly distributed  
400 between available droplets. Therefore,  $q(N)$ ,  $\beta(N)$  and  $D_v(N)$  calculated for homogeneous and  
401 extremely inhomogeneous mixing coincide with each other.

402 Numerical simulations also showed, that the effect of temperature on mixing is more  
403 pronounced for the cases when the cloud temperature is warmer than that of the entrained air, i.e.  
404  $T_1 > T_2$ , as compared to the cases with  $T_1 < T_2$ .

405

## 406 **4. Progressive mixing**

### 407 **4.1 Effect on microphysical parameters**

408 In the previous sections the mixing was considered as a single event, i.e.  $\mu$  fraction of the  
409 cloudy air mixed up with  $(1 - \mu)$  fraction of entrained dry air. Such mixing will be referred to as  
410 “primary” mixing. Primary mixing results in an ensemble of elementary volumes characterized by  
411 a set of microphysical and state parameters i.e.  $\bar{D}(\mu)$ ,  $N(\mu)$ ,  $RH(\mu)$ ,  $T(\mu)$ , etc. Each of these  
412 parameters has a functional dependence on  $\mu$ , and what is important, these parameters have  
413 functional relationships between each other.

414 In reality mixing is a continuous process. It does not stop after the primary mixing. The  
415 elementary volumes formed after primary mixing continue to progressively mix with each other.

416 The second stage of mixing will result in an ensemble of elementary volumes characterized by  
417 a set of parameters  $D_v^{(2)}$ ,  $N^{(2)}$ ,  $RH^{(2)}$ ,  $T^{(2)}$ , etc. Here the superscript <sup>(2)</sup> indicates the stage of  
418 mixing. After the second stage the mixed volumes undergo subsequent stages of mixing.

419 The idealised conceptual diagram of the progressive mixing is shown in Fig. 8. As mentioned  
420 in Sect. 2.1, the actual process of mixing is indeed much more complex than the sequence of  
421 discrete events portrayed in Fig.8. However, as it will be shown below, this simplified  
422 consideration of allows establishing main features of evolution of relationships between the

423 microphysical moments affected by mixing. The obtained results facilitates identification of type  
424 of mixing from in-situ measurements.

425 Progressive mixing was simulated with the help of a numerical model, where parcels were  
426 randomly mixed with each other and with the cloud environment. The mixing fraction  $\mu$  was also  
427 set to be random during each mixing event. Models of stochastic mixing have been used in a  
428 number of studies (e.g. Krueger et al., 1997; Su et al., 1998; Burnet and Brenguier, 2007). In the  
429 present work the analysis of progressive mixing is expanded to examine its effect on the  
430 relationship between moments of the droplet size distribution.

431 The results of the progressive mixing for the first four stages are presented in Fig. 9. As seen  
432 from Fig. 9 the functional relationship between the pairs of microphysical and state parameters  
433 exists only for the primary stage. For higher mixing stages these functional relationships break  
434 down. Thus, cloud volumes with the same  $N^{(2)}$  may have different  $D_v^{(2)}$ . Figure 9 also shows that  
435 the regions of scattering of  $q(N)$ ,  $\beta(N)$  and  $D_v(N)$  for stages 2, 3 and 4 are limited from above by  
436 the inhomogeneous mixing (red dashed lines) and from below by primary homogeneous mixing  
437 (red solid lines).

438 Figure 10 presents a conceptual  $N - q$  diagram explaining breaking the functional  
439 relationships during progressive homogeneous mixing. After the first stage of mixing the  $N - q$   
440 points will be scattered along the line  $OB$  and point  $C$ . The line  $OB$  corresponds to the ensemble of  
441 points with  $RH = 1$ . Therefore, result of mixing between two saturated volumes randomly selected  
442 on  $AB$ , will remain on the same line. Point  $C$  corresponds to the ensemble of points with  $N = 0$ ,  
443  $RH_2 \leq RH_C(\mu^{(1)}) \leq 1$ , where  $0 \leq \mu^{(1)} < \mu_{cr}$ . Therefore, mixing between point  $A$  (Fig.10) and  
444 point  $C$ , when  $RH = 1$  will result in scattering along the line  $AC$  (degenerate case). Points resulted  
445 from mixing between  $A$  ( $RH = 1$ ) and point  $C$ , when  $RH_2 \leq RH_C < 1$ , will scattered over the  
446 ensemble of dashed lines shown in Fig.10. These lines will fill the sector  $CAB$ . Random mixing  
447 between points on the line  $OB$  and  $C$ , will eventually fill the entire sector  $COB$ . The same  
448 consideration can be applied to progressive mixing between other moments.

449 During the progressive mixing  $N^{(n)}$ ,  $\beta^{(n)}$ ,  $q^{(n)}$  and  $D_v^{(n)}$  formed in the elementary parcels tend  
450 to approach those in the undiluted cloud, i.e.  $N_1$ ,  $\beta_1$ ,  $q_1$  and  $D_{v1}$ . This process can be considered as  
451 a surrogate to the diffusion process between the cloud and sub-saturated out-of-cloud environment.  
452 The convergence of  $\beta^{(n)}$ ,  $q^{(n)}$  and  $D_v^{(n)}$  during the progressive mixing can be seen in Fig. 9, where



453 the scattering of normalized  $q^{(n)}(N)$ ,  $\beta^{(n)}(N)$  and  $D_v^{(n)}(N)$  becomes denser towards the top-right  
454 corner (1,1) with the increase of the stage of mixing.

455 It is worth noting that progressive mixing with the dry air does not break the functional  
456 relationships between the moments. This case is equivalent to detrainment of cloudy environment  
457 into dry air. It can be shown that Eq.(14) remain valid at any stage of progressive homogeneous  
458 mixing with dry air only, i.e.  $N_j/N_1 = \mu^{(1)} \dots \mu^{(j-1)}\mu^{(j)}$  where  $\mu^{(j)}$  is the mixing fraction at the  $j$ -  
459 th stage of mixing. Eqs. (15)-(24) also remain valid for the progressive mixing with the dry air  
460 only.

461 As follows from Eq. (9) for the case of extreme inhomogeneous mixing the progressive mixing  
462 does not affect the functional relations between  $N^{(n)}$ ,  $\beta^{(n)}$ ,  $q^{(n)}$  and  $D_v^{(n)}$  and other microphysical  
463 parameters. These relations remain the same regardless of the actual stage of mixing. This is one  
464 of the fundamental differences between homogeneous and inhomogeneous mixing, which can be  
465 used for identification of type of mixing from in-situ measurements.

466

#### 467 **4.2 Effect on droplet size distributions**

468 Figure 11 shows modeled droplet size distributions averaged over the ensembles of elementary  
469 volumes corresponding to the first four stages of homogeneous mixing. As seen from Fig. 11a–d  
470 for the case with  $T_1 = T_2$  the droplet size distributions are broadened towards small sizes.  
471 Depending on the stage of mixing and mixing fraction  $\mu$  the size distributions formed in each  
472 elementary volume may be unimodal or multimodal. However, due to the random nature of the  
473 modal sizes formed during mixing, the average size distributions become smooth and unimodal  
474 (Fig.11a-d).

475 Broadening of droplet size distributions towards small sizes during homogeneous mixing is  
476 well known and it was demonstrated in a number of studies (e.g. Baker and Latham, 1982; Jensen  
477 and Baker, 1989; Jeffery, 2007; Kumar et al., 2013). However, if mixing results in supersaturation  
478 (section 3.4), then the droplet size distribution may broaden towards larger sizes (Fig. 11e–h). For  
479 this to occur, both the temperature difference between the cloud and the environment  $|T_1 - T_2|$  and  
480 the relative humidity of the environment  $RH_2$  must be sufficiently large. Such conditions are  
481 inherently unstable, however, this might occur in regions that have been moistened through prior  
482 cloud detrainment. Thus homogeneous mixing may result in broadening of droplet size  
483 distributions towards either smaller or larger sizes (Fig.11).

484 These results were obtained in the frame of the formalism of homogeneous and  
485 inhomogeneous mixing. The following two works in this series (Pinsky et al., 2016a, b) will discuss  
486 the broadening of polydisperse and monodisperse  $f(D)$  during both homogeneous and  
487 inhomogeneous mixing in greater details.

488

## 489 **5 Identification of type of mixing from in-situ observations**

490 The purpose of this section is to attempt identifying type of mixing based on examining  
491 relationships between basic microphysical parameters  $N$ ,  $\beta$ ,  $LWC$ ,  $D_v$  measured from in-situ.

### 492 **5.1 Expected relationships between the moments**

493 Prior proceeding with the analysis of in-situ data we summarize the results of the previous  
494 consideration on how homogeneous and extreme inhomogeneous mixing is expected to manifest  
495 itself in relationships between basic microphysical parameters, such as  $N$ ,  $\beta$ ,  $q$  and  $D_v$ .

496 For extreme inhomogeneous mixing the relationship between the pairs of  $N$ ,  $\beta$  and  $q$  are  
497 determined by linear dependences  $M_n = \alpha_{nk}M_k$  (Eq. 10) at any stage of mixing. As follows from  
498 Eq. (11) the slopes  $\alpha_{nk}$  for  $q(N)$ ,  $\beta(N)$  and  $q(\beta)$  are equal to the ratios  $q_1/N_1$ ,  $\beta_1/N_1$ , and  $q_1/\beta_1$ ,  
499 respectively, where  $N_1$ ,  $\beta_1$  and  $q_1$  correspond to undiluted adiabatic values. The values of  $N_1$ ,  $\beta_1$   
500 and  $q_1$  may vary depending on the location inside the cloud and environmental conditions at the  
501 cloud base. Thus, the adiabatic value of  $q_1$  is a function of elevation above the cloud base  $\Delta Z$ ,  
502 whereas  $N_1$  depends on the vertical velocity at the cloud base  $u_z$  and the aerosol load. Therefore,  
503 the scattering of  $q - N$  points will be aligned along an ensemble of different lines determined by  
504  $q_1/N_1$ , which are specific to different cloud volumes. The conceptual diagram of the scattering of  
505  $q - N$  measurements in a cloud with extreme inhomogeneous mixing is shown in Fig. 12a. The  
506 scatter diagrams for other moments (e.g.  $q - \beta$ ,  $N - \beta$ ) will have the similar patterns as that in Fig.  
507 12a.

508 For the case of homogeneous mixing the functional relationship between the pairs of  $N$ ,  $\beta$ ,  $q$   
509 and  $D_v$  are disrupted by a progressive mixing. As shown in Sect. 4.1 the ensemble of points of  $N$ ,  
510  $\beta$  and  $q$  will be scattered within a sector, which is limited by lines determined by Eq. (11) (extreme  
511 inhomogeneous mixing) and Eqs. (15)-(17) (primary homogeneous), respectively (Fig. 9). What is  
512 important, is that the top of the sectors for  $q(N)$  and  $\beta(N)$  correspond to points  $[N_1, q_1]$  and  
513  $[N_1, \beta_1]$ , respectively. Since  $N_1$ ,  $\beta_1$  and  $q_1$  may vary within the same cloud, it is anticipated that  
514 the  $N$ ,  $\beta$  and  $q$  measurements will be scattered within an ensemble of sectors as shown in Fig. 12b.

515 It is important to note that that during homogeneous mixing prior reaching equilibrium,  
516 functional relationships between the microphysical moments do not exist either. After the instant  
517 mixing of cloud fraction  $\mu$  with entrained air (Fig. 1b(2)),  $q_{m0} = \mu q_0$  and  $N_{m0} = \mu N_0$ . This state  
518 corresponds to point  $D$  in Fig.10. After that droplets start evaporating until liquid mixing ratio  
519 reaches point  $A$  (Fig.10), which corresponds to the equilibrium state ( $RH = 1$ ). Therefore, during  
520 evaporation time  $q - N$  points will be scattered along the line  $AD$ . Since, point  $D$  can be located  
521 anywhere on  $OC$ , the ensemble of  $q - N$  points corresponding to non-equilibrium state will fill the  
522  $COB$  area.

523 Thus, the absence of the functional relationships between the moments during homogeneous  
524 mixing may occur both during progressive mixing and during primary mixing prior reaching the  
525 equilibrium state. The evaporation time required to reach equilibrium during homogeneous mixing  
526 is discussed in details in Pinsky et al. (2016b), and it is usually limited by few tens of seconds.  
527 However, progressive mixing is not limited in time. Therefore, it is very likely that no functional  
528 relationship between microphysical parameters will be observed during in-situ measurements.

529 Fig.12 demonstrated a fundamental difference in scattering of  $q - N$  for homogeneous and  
530 extreme inhomogeneous mixing, which will be used to facilitate identification of type of mixing in  
531 the following section.

532

## 533 **5.2 Results of observations**

534 The measurements were obtained on the University of Wyoming King Air aircraft during the  
535 COPE-MED project in South-Western part of UK during July-August 2013 (Leon et al., 2016).  
536 The UW King Air was equipped with a suite of microphysical instruments, including a DMT Cloud  
537 Droplet probe (CDP), designed for measurements of droplet sizes and their concentrations in the  
538 nominal size ranges 1–50  $\mu\text{m}$ .

539 Figure 13 shows a time series of droplet concentration, extinction coefficient, liquid water  
540 content and mean volume droplet diameter measured by the CDP during transit through a  
541 convective cell on 18 July 2013. The CDP data were sampled at 10Hz, which corresponds to  
542 approximately 10m spatial averaging. Visual examination of the spatial changes of  $N$ ,  $\beta$  and  $LWC$   
543 shows strong correlation. The amplitude of changes of these parameters reaches nearly one hundred  
544 percent with respect to their maximum. Contrary to that, the spatial variations of  $\bar{D}$  and  $D_v$  are quite  
545 conservative and their values remain nearly constant. With the exception of two cloud holes

546 between 13:50:42 and 13:50:44, the amplitude of fluctuations of  $D_v$  does not exceed 8% with  
547 standard deviation of 2.2%.

548 Figure 14 shows scatter diagrams of  $LWC(N)$ ,  $\beta(N)$ ,  $LWC(\beta)$  and  $D_v(N)$  measured by the  
549 CDP during seven consecutive penetrations of the same convective cell extended over a period of  
550 approximately 19 min. One of these penetrations is shown in Fig. 13. The measurements were  
551 conducted at  $H = 5500\text{m}$  and  $T = -12^\circ\text{C}$ . The relative humidity of the ambient air was  
552 approximately 20%. At the beginning of the sampling no precipitation size particles were observed  
553 in the cloud. However, by the end of the sampling period some raindrops and ice crystals were  
554 present in the cloud. Despite the presence of some precipitation size particles, the scatter diagrams  
555 in Fig. 14a, b and d demonstrate high correlation between pairs  $N$ ,  $\beta$  and  $LWC$ . The mean volume  
556 diameter in Fig. 14c shows very little changes from 19 to 17  $\mu\text{m}$  when concentration changes from  
557 1100 to 500  $\text{cm}^{-3}$ , However, for  $N < 200 \text{ cm}^{-3}$ , the volume diameter decreases to 12–15  $\mu\text{m}$ .

558 Red lines in Fig. 14 indicate  $q(N)$ ,  $\beta(N)$ ,  $LWC(\beta)$  and  $D_v(N)$  calculated for the 1<sup>st</sup> stage of  
559 homogeneous mixing. The calculations were performed for a monodisperse  $f(D)$  with  $D_1=18.5\mu\text{m}$ ,  
560  $N_1 = 1100 \text{ cm}^{-3}$ , and state parameters as during the measurements. Comparisons of dependences  
561  $q(N)$ ,  $\beta(N)$ ,  $LWC(\beta)$  and  $D_v(N)$  based on in-situ measurements with those obtained from  
562 numerical simulations of homogeneous mixing show minor difference for high concentrations 700  
563  $\text{cm}^{-3} < N < 1100 \text{ cm}^{-3}$  (Fig. 14a–c). Simulation also shows that for this specific case the difference  
564 between homogeneous and inhomogeneous mixing does not exceed 10% when  $700 \text{ cm}^{-3} < N <$   
565  $1100 \text{ cm}^{-3}$ . Such difference remains within the errors of measurements. Therefore, in this specific  
566 cloud for the regions with  $N > 700 \text{ cm}^{-3}$  the type of mixing cannot be unambiguously identified  
567 from the analysis of the dependences  $LWC(N)$ ,  $\beta(N)$ ,  $LWC(\beta)$  and  $D_v(N)$ . This is consistent with  
568 the assessment of feasibility of segregation of homogeneous and inhomogeneous mixing in Fig.3  
569 (dashed line). Since for homogeneous mixing  $N \propto \mu$ , than Fig.3 suggests good separation of the  
570 moments for  $N > 700 \text{ cm}^{-3}$ .

571 For the regions with  $N < 500 \text{ cm}^{-3}$  the deviation between homogeneous mixing simulations  
572 and in-situ measurements in Fig.14 becomes well pronounced and it extends beyond possible errors  
573 of measurements. This suggests that the mixing in these regions is dominated by the extreme  
574 inhomogeneous type.

575 Figure 15 shows the same type of diagrams as in Fig. 14, which were measured during 45  
576 consecutive traverses through an ensemble of deep convective cells. The sampling altitude varied

577 in the range  $3000\text{m} < H < 4500\text{m}$ , temperature  $-11^\circ\text{C} < T < 0^\circ\text{C}$ , relative humidity in the vicinity  
578 of clouds  $15\% < \text{RH} < 65\%$ . The cloud measurements were extended over a period of 2 h 13 m,  
579 which is suggestive that the convective cells were sampled at different stages of their lifetime. At  
580 the sampling level the concentration of raindrops varied from zero to few per liter, and their  
581 diameter did not exceed 2mm.

582 What is interesting that the scattering of the measurements  $LWC(N)$ ,  $\beta(N)$  and  $LWC(\beta)$  (Fig.  
583 15a, b and d) is limited by the sector, which originates from the zero point as in Fig.12a. Analysis  
584 of the measurements showed that the data points  $LWC(N)$ ,  $\beta(N)$ ,  $LWC(\beta)$  in each individual  
585 cloud traverse are well aligned along the lines with different slopes (e.g. Fig.14). After averaging  
586 over the ensemble of clouds, the area of the scattered points turned out to be located inside a sector  
587 limited by the lines with smallest and largest slopes.

588 Comparisons of the scatterdiagrams  $LWC(N)$ ,  $\beta(N)$  and  $LWC(\beta)$  in Figs.14 and 15 with the  
589 conceptual diagrams in Fig.12 unambiguously suggest that interaction between cloud and  
590 environment in the studied clouds was dominated by inhomogeneous mixing. It should be  
591 emphasized that analysis of a stand alone mixing diagram  $N - D_v$  would not allow unambiguously  
592 draw such conclusion.

593

## 594 **6. Discussion**

595 One of the assumptions in most past studies is that for a sequence of the cloud samples  
596 collected along the flight path, the adiabatic values of  $N_1$ ,  $q_1$ ,  $\beta_1$ ,  $D_1$  and environmental parameters  
597  $e_2$  and  $T_2$  remain the same. In fact these parameters may vary both within the same cloud or  
598 sequence of samples clouds, and the amplitude of their variations depends on microphysical and  
599 thermodynamical properties inside and outside the cloud environment. This variation will result in  
600 an ensemble of relationships  $M_n = F_{nk}(M_k)$ , and enhance scattering of the data points. In such  
601 cases identification of the type of mixing based on the  $N - D_v$  diagram may result in confusion  
602 between homogeneous and inhomogeneous mixing. As demonstrated in Sect. 5, consideration of  
603  $N - q$  and  $N - \beta$  diagrams may provide a better identification type of mixing.

604 Strictly speaking the identification of type of mixing from particle probe measurements as it  
605 was performed in Sect. 5 is incomplete. It allows establishing correlation between microphysical  
606 moments and makes a formal conclusion about the mixing type, however it does not allow  
607 judgement about stage of mixing (i.e. whether mixing is complete by reaching equilibrium). In

608 most previous studies, including this one, identification of type of mixing was based on the  
609 assumption that the sampled cloud volume is in equilibrium state ( $RH = 1$ ), and that it reached the  
610 final stage of mixing (Fig.1 a2, a3, b3). It is possible that at the moment of measurement the process  
611 of mixing is not complete and the droplet free filaments remained undersaturated (Fig.1 a1, b1,  
612 b2). In this case the relationship between different moments may be well described as  $M_n =$   
613  $\alpha_{nk}M_{nk}$  and the mixing be confused with inhomogeneous mixing.

614 In order to identify stage of mixing, high frequency collocated measurements of temperature  
615 and humidity are required. Unfortunately current technology does not allow such measurements  
616 yet.

617 Identification of type of mixing from in-situ observations is based on examination of  
618 relationships between moments of the size distributions measured along the flight path. The basic  
619 assumption underlying this analysis is that the cloud environment is not affected by other non-  
620 adiabatic processes.

621 Thus, collision-coalescence, riming or Wegener-Bergeron-Findeisen processes may change  
622 the droplet number concentration and liquid water content, and therefore, affect the relationship  
623 between the moments. Activation of interstitial CCN will result in breaking correlation between  
624 the moments due to formation of large concentration of droplets. Broad size distributions may also  
625 hinder identification of type of mixing due to partial evaporation of small droplets (Pinsky et al.  
626 2016a)

627 It is anticipated that most suitable candidates to study mixing-entrainment process are non-  
628 precipitating convective clouds and stratocumulus clouds with relatively narrow droplet size  
629 distributions.

630 Another limiting factor is that the above consideration did not account for the effect of  
631 changing humidity in a vertically ascending parcel. Thus in droplet free entrained air relative  
632 humidity increases approximately 10% for  $\Delta z = 200\text{m}$  at  $T = 0^\circ\text{C}$ . After reaching saturation the  
633 mixing turns into a degenerate case, which will appear as extreme inhomogeneous mixing. Joint  
634 effects of evaporating droplets and an increase in  $S$  during the vertical ascent may facilitate  
635 reaching saturation state. This case may also be relevant to the convective cloud described in  
636 Sect.5.2.

637

638

## 7. Conclusions

This study analyzes dependences of different moments of  $f(D)$  in the frame of formalism of homogeneous and extremely inhomogeneous mixing. The analysis was performed for the final stage of mixing based on the mass and energy conservation consideration. The following results were obtained in the frame of this study:

1. Simple analytical relationships between the main microphysical moments were obtained for the final state homogenous and extreme inhomogeneous mixing.

2. It was shown that the functional relationships between the moments exist only for the first stage of homogeneous mixing, when equilibrium is reached. Subsequent progressive homogeneous mixing breaks the functional relationship between the moments.

3. It was demonstrated that consideration of scattering  $N - LWC$ ,  $N - \beta$  diagrams facilitates identification of type of mixing from in-situ measurements. For extreme inhomogeneous mixing the scattering of the data points  $N - LWC$ ,  $N - \beta$  will be limited by a sector originating at zero point (Fig.12a). However, for homogeneous mixing the scattering data points will be limited by a sector originating at  $(N_1, LWC_1)$  and  $(N_1, \beta_1)$  (Fig.12b). Utilizing a stand-alone conventional  $N - D_v$  mixing diagram may not provide unambiguous answer about type of mixing.

4. The developed approach was applied to a set of in-situ measurements collected in convective clouds. The analysis of the dependences between  $N$ ,  $\beta$ ,  $LWC$  and  $D_v$  suggests that the interaction between entrained and cloudy environments for the studied clouds was dominated by inhomogeneous mixing.

The present study considers relationships between different moments of  $f(D)$  for the final stage of mixing. The following two works Pinsky et al. (2016a, b) in this series provide a detailed analysis of time dependences of droplet size distributions and its moments during homogeneous and inhomogeneous mixing.

*Acknowledgement.* The authors appreciate two anonymous reviewers for their comments. Alexei Korolev work was supported by Environment Canada and Transport Canada. The COPE-MED project was funded by National Science Foundation grant AGS-1230292 and AGS-1230203. The contribution of Mark Pinsky and Alex Khain was supported by the Israel Science Foundation (grant 1393/14), the Office of Science (BER), US Department of Energy Award DE-SC0006788 and the Binational US-Israel Science foundation (grant 2010446).

670

671 **Appendix A: Liquid water deficit**

672 The objective of this section is to find the amount of liquid water, which is required to be  
 673 evaporated in order to saturate the parcel formed after mixing. Assume that  $q_{v1}$ ,  $q_{v2}$  are the mixing  
 674 vapor ratios in the cloudy and entrained parcels, respectively, and  $T_1$ ,  $T_2$  are their respective initial  
 675 temperatures. First, we find the saturation ratio  $S_{m0}$  formed after instant mixing of the cloud and  
 676 entrained before the cloud droplets start evaporating.

677 The vapor mixing ratio  $q_{vm}$  formed in the mixed volume will be

$$678 \quad q_{vm} = \mu q_{v1} + (1 - \mu) q_{v2} \quad (\text{A1})$$

679 The vapor pressure  $e_m$  in the mixed volume can be derived from Eq. (A1) by substituting

$$680 \quad q_v = \frac{e}{p - e} \frac{R_a}{R_v}, \text{ i.e.}$$

$$681 \quad e_m = p \frac{\mu + \frac{e_2(p - e_1)}{p(e_1 - e_2)}}{\mu + \frac{(p - e_1)}{(e_1 - e_2)}} \quad (\text{A2})$$

682 The temperature of the mixed volume  $T_{m0}$  can be found from the energy conservation law

$$683 \quad \mu(q_{v1}c_{pv} + c_{pa})(T_1 - T_{m0}) = (1 - \mu)(q_{v2}c_{pv} + c_{pa})(T_{m0} - T_2) \quad (\text{A3})$$

684 here  $c_{pv}$ ,  $c_{pa}$  are the specific heat capacitance of water vapor and dry air at constant pressure,  
 685 respectively,  $T_1$ ,  $T_2$  are the initial temperatures in the first and second parcels before mixing.  
 686 Substituting  $q_{v1}$ ,  $q_{v2}$  yields the temperature in the mixed volume

$$687 \quad T_{m0} = \frac{\mu T_1 + \alpha(1 - \mu)T_2}{\mu + \alpha(1 - \mu)} \quad (\text{A4})$$

688 here

$$689 \quad \alpha = \frac{1 + \frac{c_{pv}R_a e_2}{c_{pa}R_v(p - e_2)}}{1 + \frac{c_{pv}R_a e_1}{c_{pa}R_v(p - e_1)}} \quad (\text{A5})$$

690 With a good accuracy  $\alpha \cong 1$ . The resulting relative humidity after mixing the two volumes  
 691 will be



692 
$$RH_{m0} = \frac{e_{m0}}{e_s(T_{m0})} \quad (\text{A6})$$

693 where  $e_s(T_{m0})$  is the saturated vapor pressure at temperature  $T_{m0}$ .

694 The process of evaporation is accompanied by changing humidity and temperature due to  
 695 latent heat of vaporization. This process is described by the Eq. (C2) in Korolev and Mazin (2003).  
 696 Assuming the process to be isobaric (i.e. vertical velocity  $u_z = 0$ ) and absence of ice ( $dq_i = 0$ ),  
 697 Eq. (C2) (Korolev and Mazin, 2003) yields

698 
$$\frac{dS}{S+1} = \left( \frac{1}{S+1} \frac{pR_v}{e_s R_a} + \frac{L^2}{c_{pa} R_v T^2} \right) dq \quad (\text{A7})$$

699 Integrating Eq. (A7) from initial  $S_{m0}$  to saturation state, when  $S = 0$ , and taking into account  
 700 that  $RH = S + 1$ , gives

701 
$$\delta q_m = -b \ln \left( \frac{1 + aRH_{m0}}{1 + a} \right) \quad (\text{A8})$$

702 the mixing ratio of liquid water required to evaporate in order to saturate 1kg of the cloud volume  
 703 formed after mixing with the entrained air, but before droplet start evaporating. Here  $a = \frac{E_s R_a L^2}{p c_p R_v^2 T_m^2}$ ,

704 
$$b = \frac{c_p R_v T_m^2}{L^2}.$$

705 Since  $\left| \frac{A(RH_{m0}-1)}{1+A} \right| < 1$ , Eq.(A8) can be simplified as

706 
$$\delta q_m = ab \frac{1 - RH_{m0}}{1 + a} = -\frac{S_{m0}}{A_2} \quad (\text{A9})$$

707 where  $A_2 = \frac{ab}{1+a}$ . The analysis of Eqs. (A8)-(9) shows that for wide range of temperatures  $-30 \text{ }^\circ\text{C} <$   
 708  $T < 30 \text{ }^\circ\text{C}$ , both equations hold with high accuracy as long as the temperatures of the sub-saturated  
 709 and cloud parcels  $|T_1 - T_2| < 10^\circ\text{C}$ .

710 Figure A1 shows comparisons of modeled  $\delta q_m$  and that calculated from Eqs. (A8) and (A9)  
 711 for three different temperatures. The model solved a system of differential equation with  
 712 incremental evaporation of liquid water until saturation is reached. As seen from Fig. A1 the  
 713 agreement between modeled  $\delta q_m$  and that calculated from Eq. (A8)-(A9) is quite good and does  
 714 not exceed few percent at  $RH_{m0} = 0.5$ . This discrepancy results from assumption that  $e_s$  and  $T$  are  
 715 constant in Eqs.(A8)-(A9).

716

717 **Appendix B: Liquid water deficit when  $T_1 = T_2$**

718 Eq.(A2) by assuming that  $p \gg e_1$  and  $p \gg e_2$  can be simplified as

719 
$$e_{m0} = \mu e_1 + (1 - \mu)e_2 \quad (\text{B2})$$

720 As follows from Eq.(A4) for the case  $T_1 = T_2$  with high accuracy  $T_{m0} = T_1 = T_2$ . Therefore,  
721  $e_s(T_{m0}) = e_s(T_1) = e_s(T_2)$ . Dividing Eq.(B1) by  $e_s$  yields

722 
$$RH_{m0} = \mu RH_1 + (1 - \mu)RH_2 \quad (\text{B3})$$

723 In most liquid clouds  $RH_1 = 1$  (Korolev and Mazin 2003). Therefore, Eq.B2 turns into

724 
$$RH_{m0} = \mu + (1 - \mu)RH_2 \quad (\text{B4})$$

725 Substituting Eq.(B4) in Eq.(B1) yields

726 
$$\delta q_m = -b \ln \left( 1 + \frac{a(1 - \mu)(RH_2 - 1)}{1 + a} \right) \quad (\text{B5})$$

727 The expression under logarithm can be presented as the first two terms of the series expansion  
728 of  $\left( 1 + \frac{a(RH_2 - 1)}{1 + a} \right)^{(1 - \mu)}$ . Substituting this expression into Eq.(B5), gives

729 
$$\delta q_m = (1 - \mu)\delta q^* \quad (\text{B6})$$

730 where

731 
$$\delta q^* = -b \ln \left( \frac{1 + aRH_2}{1 + a} \right) \quad (\text{B7})$$

732 is the mixing ratio of liquid water required to saturate 1 kg of the entrained dry volume.

733

734 **Appendix C: Temperature in the mixing volume**

735 The energy conservation for evaporating droplets can be written as

736 
$$(T - T_{m0})(1 + q_{vm})c_{pm} + (1 - \mu)\delta q^* L = 0 \quad (\text{C1})$$

737 here  $c_{pm}$  is the specific heat capacity of the moist air

738 
$$c_{pm} = \frac{c_{pa} + q_{vm}c_{pv}}{1 + q_{vm}} \quad (\text{C2})$$

739 Since  $q_{vm} \ll 1$  and,  $c_{pa} \cong c_{pm}$  Eq.(C1) may be simplified, so that the final temperature after  
740 mixing

741 
$$T = T_{m0} - \frac{(1 - \mu)\delta q^* L}{c_{pa}} \quad (\text{C3})$$

742 For the case when  $T_1 \neq T_2$  Eq. (C3) should be replaced by

$$743 \quad T = T_{m0} - \frac{\delta q_m L}{c_{pa}} \quad (C4)$$

744 Eqs. (C3) and (C4) are valid for the mixing fraction  $\mu > \mu_{cr}$ . For  $\mu \leq \mu_{cr}$  all entrained liquid  
745 water  $\mu q_0$  evaporates, and the final temperature will be

$$746 \quad T = T_{m0} - \frac{\mu q_0 L}{c_{pa}} \quad (C5)$$

747

## 748 **References**

- 749 Andrejczuk M., Grabowski, W. W., Malinowski, S. P., and Smolarkiewicz, P. K.: Numerical  
750 simulation of cloud–clear air interfacial mixing: homogeneous vs. inhomogeneous mixing., J.  
751 Atmos. Sci., 66, 2493-2500, 2009.
- 752 Baker, M. B. and Latham, J.: The evolution of droplet spectra and the rate of production of  
753 embryonic raindrops in small cumulus clouds, J. Atmos. Sci., 36, 1612–1615, 1979.
- 754 Baker, M. B. and Latham, J.: A diffusive model of the turbulent mixing of dry and cloudy air, Q.  
755 J. R. Met. Soc., 108, 871–898, 1982.
- 756 Baker, M. B., Corbin, R. G., and Latham, J.: The influence of entrainment on the evolution of cloud  
757 droplet spectra: I. A model of inhomogeneous mixing, Q. J. Roy. Meteor. Soc., 106, 581–598,  
758 1980.
- 759 Beals, M.J., and Fugal, J.P., Shaw, R.A., Lu, J., Spuler, S.M., Stith, J.L.: Holographic  
760 measurements of inhomogeneous cloud mixing at the centimeter scale. Science, 350, 87-90,  
761 2015
- 762 Bohren, C. F. and Albrecht, C. H.: Atmospheric Thermodynamics, Oxford University Press, New  
763 York, 402 pp., 1998.
- 764 Bower, K. N. and Choulaton, T. W.: The effects of entrainment on the growth of droplets in  
765 continental cumulus clouds, Q. J. Roy. Meteor. Soc., 114, 1411–1434, 1988.
- 766 Broadwell, J. E., and R. E. Breidenthal: A simple model of mixing and chemical reaction in a  
767 turbulent shear layer. J. Fluid Mech., 125, 397–410, 1982
- 768 Burnet, F. and Brenguier, J. L.: Observational study of the entrainment-mixing process in warm  
769 convective clouds, J. Atmos. Sci., 64, 1995–2011, 2007.

770 Devenish, B. J., Bartello, P., Brenguier, J.-L., Collins, L. R., Grabowski, W. W., Ijzermans, R. H.  
771 A., Malinovski, S. P., Reeks, M.W., Vassilicos, J. C., Wang, L- P., and Warhaft, Z.: Droplet  
772 growth in warm turbulent clouds, *Q. J. Roy. Meteor. Soc.*, 138, 1401–1429, 2012.

773 Dimotakis, P. E.: Turbulent mixing, *Annu. Rev. Fluid Mech.*, 37, 329–356, 2005.

774 Gerber, H., Frick, G., Jensen, J. B., and Hudson, J. G.: Entrainment, mixing, and microphysics in  
775 trade-wind cumulus, *J. Meteorol. Soc. Jpn.*, 86, 87–106, 2008.

776 Hill, T. A. and Choulaton, T. W.: An airborne study of the microphysical structure of cumulus  
777 clouds, *Q. J. Roy. Meteor. Soc.*, 111, 517–544, 1985.

778 Jeffery, C. A.: Inhomogeneous cloud evaporation, invariance, and Damköhler number, *J. Geoph.*  
779 *Res.*, 112, D24S21, doi:10.1029/2007JD008789, 2007.

780 Jarecka, D., Grabowski, W. W., Morrison, H., Pawlowska, H.: Homogeneity of the Subgrid-Scale  
781 Turbulent Mixing in Large-Eddy Simulation of Shallow Convection. *J. Atmos. Sci.* 70, 2751-  
782 2767, 2013

783 Jensen, J. and Baker, M.: A simple model of droplet spectra evolution during turbulent mixing, *J.*  
784 *Atmos. Sci.*, 46, 2812–2829, 1989.

785 Korolev A. V.: The influence of supersaturation fluctuations on droplet spectra formation. *Journal*  
786 *of the Atmospheric Sciences*, 52, 3620-3634, 1995.

787 Korolev, A. V. and Isaac, G. A.: Drop growth due to high supersaturation caused by isobaric  
788 mixing, *J. Atmos. Sci.*, 57, 1675–1685, 2000.

789 Korolev, A. V. and I.P. Mazin,: Supersaturation of water vapor in clouds. *J. Atmos. Sci.*, 60, 2957-  
790 2974, 2003.

791 Krueger, S., Su, C.-W., and McMurtry, P.: Modeling entrainment and finescale mixing in cumulus  
792 clouds, *J. Atmos. Sci.*, 54, 2697–2712, 1997.

793 Kumar, B., Schumacher, J., and Shaw, R. A.: Cloud microphysical effects of turbulent mixing and  
794 entrainment, *Theor. Comput. Fluid Dyn.*, 27, 361–376, 2013.

795 Lasher-Trapp, S. G., Cooper, W. A., and Blyth, A. M.: Broadening of droplet size distributions  
796 from entrainment and mixing in a cumulus cloud, *Q. J. Roy. Meteor. Soc.*, 131, 195–220, 2005.

797 Latham, J. and Reed, R. L.: Laboratory studies of the effects of mixing on the evolution of cloud  
798 droplet spectra, *Q. J. Roy. Meteor. Soc.*, 103, 297–306, 1977.

799 Lehmann, K., Siebert, H., and Shaw, R. A.: Homogeneous and inhomogeneous mixing in cumulus  
800 clouds: dependence on local turbulence structure, *J. Atmos. Sci.*, 66, 3641–3659, 2009.

801 Leon, D. C., French, J. R., Lasher-Trapp, S., Blyth, A. M., Abel, S. J., Ballard, S., Bennett, L. J.,  
802 Bower, K., Brooks, B., Brown, P., Choullarton, T., Clark, P., Collier, C., Crosier, J., Cui, Z.,  
803 Dufton, D., Eagle, C., Flynn, M. J., Gallagher, M., Hanley, K., Huang, Y., Kitchen, M., Korolev,  
804 A., Lean, H., Liu, Z., Marsham, J., Moser, D., Nicol, J., Norton, E. G., Plummer, D. Price, J.,  
805 Ricketts, H., Roberts, N., Rosenberg, P. D., Taylor, J. W., Williams, P. I., and Young, G.: The  
806 Convective Precipitation Experiment (COPE): investigating the origins of heavy precipitation  
807 in the southwestern UK, *B. Am. Meteorol. Soc.*, in press, 2016.

808 Lu, C., and Liu Y., Niu, S.: Examination of turbulent entrainment mixing mechanisms using a  
809 combined approach. *J. Geophys. Res.*, 116, D20207, 2011.

810 Paluch, I. R.: Mixing and the droplet size spectrum: generalizations from the CCOPE data, *J.*  
811 *Atmos. Sci.*, 43, 1984–1993, 1986.

812 Paluch, I. R. and Baumgardner, D. G.: Entrainment and fine-scale mixing in a continental  
813 convective cloud, *J. Atmos. Sci.*, 46, 261–278, 1989.

814 Paluch, I. R. and Knight, C. A.: Mixing and evolution of cloud droplet size spectra in a vigorous  
815 continental cumulus, *J. Atmos. Sci.*, 41, 1801–1815, 1984.

816 Pinsky, M., Khain, A., Korolev, A., and Magaritz-Ronen, L.: Theoretical investigation of mixing  
817 in warm clouds – Part 2: Homogeneous mixing, *Atmos. Chem. Phys. Discuss.*, 15, 30269-  
818 30320, doi:10.5194/acpd-15-30269-2015, 2015.

819 Pinsky, M., Khain, A., and Korolev, A.: Theoretical analysis of mixing in liquid clouds – Part 3:  
820 Inhomogeneous mixing, *Atmos. Chem. Phys. Discuss.*, 15, 30321–30381, doi:10.5194/acpd-  
821 15-30321-2015, 2015.

822 Pinsky, M., Khain, A., Korolev, A., and Magaritz-Ronen, L.: Theoretical investigation of mixing  
823 in warm clouds – Part 2: Homogeneous mixing, *Atmos. Chem. Phys.*, submitted, 2016

824 Pinsky, M., Khain, A., and Korolev, A.: Theoretical analysis of mixing in liquid clouds – Part 3:  
825 Inhomogeneous mixing, *Atmos. Chem. Phys. Submitted*, 2016

826 Rogers, R. R.: *A Short Course in Cloud Physics*, Pergamon press, Oxford, 227 pp., 1976.

827 Squires, P.: The growth of cloud drops by condensation. *Aust. J. Sci. Res.*, 5, 66–86, 1952.

828 Su, C.-W., Krueger, S. K., McMurtry, P. A., and Austin, P. H.: Linear eddy modeling of droplet  
829 spectral evolution during entrainment and mixing in cumulus clouds, *Atmos. Res.*, 47-48, 41-  
830 58, 1998.

831 **Table 1**832 **List of Symbols**

Symbol	Description	Units
$A_2$	$\frac{pR_v}{e_s R_a} + \frac{L^2}{c_{pa} R_v T^2}$	-
$a$	$\frac{e_s R_a L^2}{p c_{pa} R_v T^2}$	-
$b$	$\frac{c_{pa} R_v T^2}{L^2}$	-
$c_{pa}$	specific heat capacity of dry air at constant pressure	$\text{J kg}^{-1}\text{K}^{-1}$
$c_{pv}$	specific heat capacity of water vapor at constant pressure	$\text{J kg}^{-1}\text{K}^{-1}$
$\bar{D}$	mean droplet diameter	m
$D_2$	mean square droplet diameter	m
$D_v$	mean volume droplet diameter	m
$e$	water vapor pressure	$\text{N m}^{-2}$
$e_1$	initial water vapor pressure in the cloud parcel	$\text{N m}^{-2}$
$e_2$	initial water vapor pressure in the entrained sub-saturated parcel	$\text{N m}^{-2}$
$e_s$	saturation vapor pressure above flat surface of water	$\text{N m}^{-2}$
$f(D)$	size distribution of cloud droplets normalized on unity	$\text{m}^{-1}$
$L$	latent heat for liquid water	$\text{J kg}^{-1}$
$M_n$	$n$ -th moment of the droplet size distribution	$\frac{\int_0^{\infty} f(r)r^n dr}{\int_0^{\infty} f(r)dr}$ $\text{m}^n$
$N$	concentration of droplets	$\text{m}^{-3}$
$N_1$	concentration of droplets before mixing	$\text{m}^{-3}$
$p$	pressure of moist air	$\text{N m}^{-2}$
$R_a$	specific gas constant of moist air	$\text{J kg}^{-1}\text{K}^{-1}$
$R_v$	specific gas constant of water vapor	$\text{J kg}^{-1}\text{K}^{-1}$
$RH$	$e/E_s$ , relative humidity over water (saturation ratio)	-

$RH_1$	initial relative humidity in the cloud volume ( $RH_1=1$ )	-
$RH_2$	relative humidity in the entrained sub-saturated parcel	-
$RH_{m0}$	relative humidity after instant mixing of cloudy and entrained air but before droplets evaporation	-
$q$	cloud liquid water mixing ratio (mass of liquid water per 1kg of dry air)	-
$q_1$	cloud liquid water mixing ratio before mixing	-
$q_v$	water vapor mixing ratio (mass of water vapor per 1kg of dry air)	-
$S$	$e/e_s - 1$ , supersaturation	-
$S_2$	supersaturation of the dry out-of-cloud air	-
$S_{m0}$	supersaturation after instant mixing of cloudy and entrained air, but before droplets start evaporating	-
$T$	temperature	K
$T_1$	temperature of the cloud parcel before mixing	K
$T_2$	temperature of the entrained sub-saturated parcel before mixing	K
$T_{m0}$	temperature of the parcel after vapor mixing, but before droplet evaporation	K
$\beta$	extinction coefficient	$m^{-1}$
$\beta_1$	extinction coefficient before mixing	$m^{-1}$
$\delta q_m$	mixing ratio of liquid water required to saturate 1kg of the cloud volume after instant mixing, but before droplet evaporation.	-
$\delta q^*$	mixing ratio of liquid water required to saturate 1kg of the dry out-of-cloud air	-
$\mu$	cloud fraction of mixing air, $0 \leq \mu \leq 1$	-
$\mu_{cr}$	critical cloud fraction, such that for $\mu \leq \mu_{cr}$ all droplets evaporate	-
$\rho_a$	density of the dry air	$kg\ m^{-3}$
$\rho_w$	density of liquid water	$kg\ m^{-3}$
$\xi$	coefficient $0 \leq \xi \leq 1$ characterizing proximity of homogeneous mixing to inhomogeneous ( when $\xi \rightarrow 0$ ).	-

834 **Figure Captions**

835 **Figure 1.** Classical conceptual diagram of (a) inhomogeneous and (b) homogeneous mixing. 1  
836 initial state; 2 mixing state; 3 final state.

837 **Figure 2.** Dependence of critical mixing fraction  $\mu_{cr}$  versus mixing ratio  $q_0$  calculated from Eq.(7).  
838 Circles indicate modeled points. The calculations were performed for  $T=0C$  and  
839  $H=3000m$ .

840 **Figure 3.** Dependence of  $\xi$  versus  $\mu$ . Numbers are the dimensionless ratios  $\delta q^*/q_1$ . Critical mixing  
841 ratios  $\mu_{cr}$  are indicated by stars. Grey area indicates area where the moments of  
842 homogeneous and extreme inhomogeneous mixing may not be segregated from in-situ  
843 measurements. Dashed line was calculated for the cloud in Figs.13-14.

844 **Figure 4.** Simulation of (a) liquid water mixing ratio, (b) droplet number concentration, (c) integral  
845 droplet diameter, (d) extinction coefficient, (e) mean volume diameter, (f) time of phase  
846 relaxation, (g) relative humidity in the mixed volume before droplet evaporation  $RH_{m0}$   
847 and at the equilibrium state  $RH_m$ , (h) final temperature  $T_{m0}$  versus ratio of mixing  $\mu$   
848 formed after homogeneous and extreme inhomogeneous mixing between dry and cloudy  
849 parcel with monodisperse droplets. Black stars indicate critical mixing fraction  $\mu_{cr}$   
850 calculated from Eq.(7). The calculations were performed for  $RH_2 = 0.2, 0.5, 0.8, 0.95$ ;  
851  $D_1=20\mu m, N_1=500cm^{-3}; T_1 = T_2 = 0C; H=1000m$ .

852 **Figure 5.** Dependence of normalized liquid water mixing ratio  $q/q_1$  (a,d,g), extinction coefficient  
853  $\beta/\beta_1$  (b,e,h) and mean volume diameter  $D_v/D_{v1}$  (c,f,j) versus normalized number  
854 concentration  $N/N_1$  for various humidity of the entrained air (a,b,c), for various liquid  
855 water mixing ratios (d,e,f) and for various temperatures (g,h,j). The calculations were  
856 performed the initial conditions:  $H=1000m, D_1=20\mu m$ ; for (a-c; g-j)  $N_1=500cm^{-3}$ ; for (a-  
857 f)  $T_1 = T_2 = 0C$ .

858 **Figure 6.** Simulation of (a) droplet number concentration and (b) liquid water mixing ratio, (c)  
859 integral droplet diameter, (d) extinction coefficient, (e) mean volume diameter, (f) time of  
860 phase relaxation, (g) relative humidity in the mixed volume before droplet evaporation  
861  $RH_{m0}$  and at the equilibrium state  $RH_m$ , (h) final temperature  $T_m$  versus ratio of mixing  
862  $\mu$  formed after homogeneous and extreme inhomogeneous mixing between dry and cloudy



863 parcel with monodisperse droplets. The calculations were performed for  $RH_2=0.9$ ;  
864  $D_1=10\mu\text{m}$ ,  $N_1=500\text{cm}^{-3}$ ;  $T_1 = 0\text{C}$ ;  $T_2 = -10\text{C}, -5\text{C}, 0\text{C}$ ;  $H=1000\text{m}$ .

865 **Figure 7.** Effect of temperature difference between cloud and entrained air on mixing. The  
866 calculations were performed for initial temperatures  $T_2$ : (1)  $-10\text{C}$ ; (2)  $-5\text{C}$ ; (3)  $0\text{C}$ . Grey  
867 circles indicate extremely inhomogeneous mixing on line 1 at the  $AB$  interval. The rest  
868 cases on extremely inhomogeneous mixing are indicated by open circles. The initial  
869 conditions used for the calculations were:  $H=1000\text{m}$ ,  $RH_2=90\%$ ;  $D_1 = 10\mu\text{m}$ ,  $N_1 = 500\text{cm}^{-3}$ ,  
870  $T_1=0\text{C}$ .

871 **Figure 8.** Conceptual diagram of cascade mixing of the out-of-cloud entrained parcel with the  
872 cloudy environment

873 **Figure 9.** Simulation of stochastic mixing corresponding to stages 1-4 as indicated in Fig.8. Solid  
874 red lines indicate the normalized dependences  $q$ ,  $\beta$ ,  $D_v$  vs.  $N$  for the primary stage of  
875 homogeneous mixing. Dashed red lines indicate the same dependences for  
876 inhomogeneous mixing. The initial conditions used for the simulations were:  $H=1000\text{m}$ ,  
877  $T_1 = T_2 = 0\text{C}$ ;  $RH_2=0.5$ ;  $D_1 = 10\mu\text{m}$ ,  $N_1 = 500\text{cm}^{-3}$ .

878 **Figure 10.** Conceptual diagram explaining breaking the functional relationships between the  
879 microphysical moment during progressive missing (see text).

880 **Figure 11.** Droplet size distributions formed during the progressive homogeneous mixing  
881 corresponding to the (a,e) primary stage; (b,f) 2<sup>nd</sup> stage; (c,g) 3<sup>rd</sup> stage; (d,h) 4<sup>th</sup> stage. Left  
882 column (a,b,c,d) corresponds to the case, when the cloud temperature is equal to the dry  
883 air temperature  $T_1 = T_2 = 0\text{C}$ ; right column (e,f,g,h) corresponds to the case when  $T_1 =$   
884  $0\text{C}$ ,  $T_2 = -10\text{C}$ . For both cases the simulation was performed for  $D_1 = 10\mu\text{m}$ ;  $N=500\text{cm}^{-3}$ ;  
885  $RH_2=0.9$ .

886 **Figure 12.** Conceptual diagrams of scattering of measurements of  $q$  versus  $N$  for (a) extreme  
887 inhomogeneous and (b) homogeneous mixing.

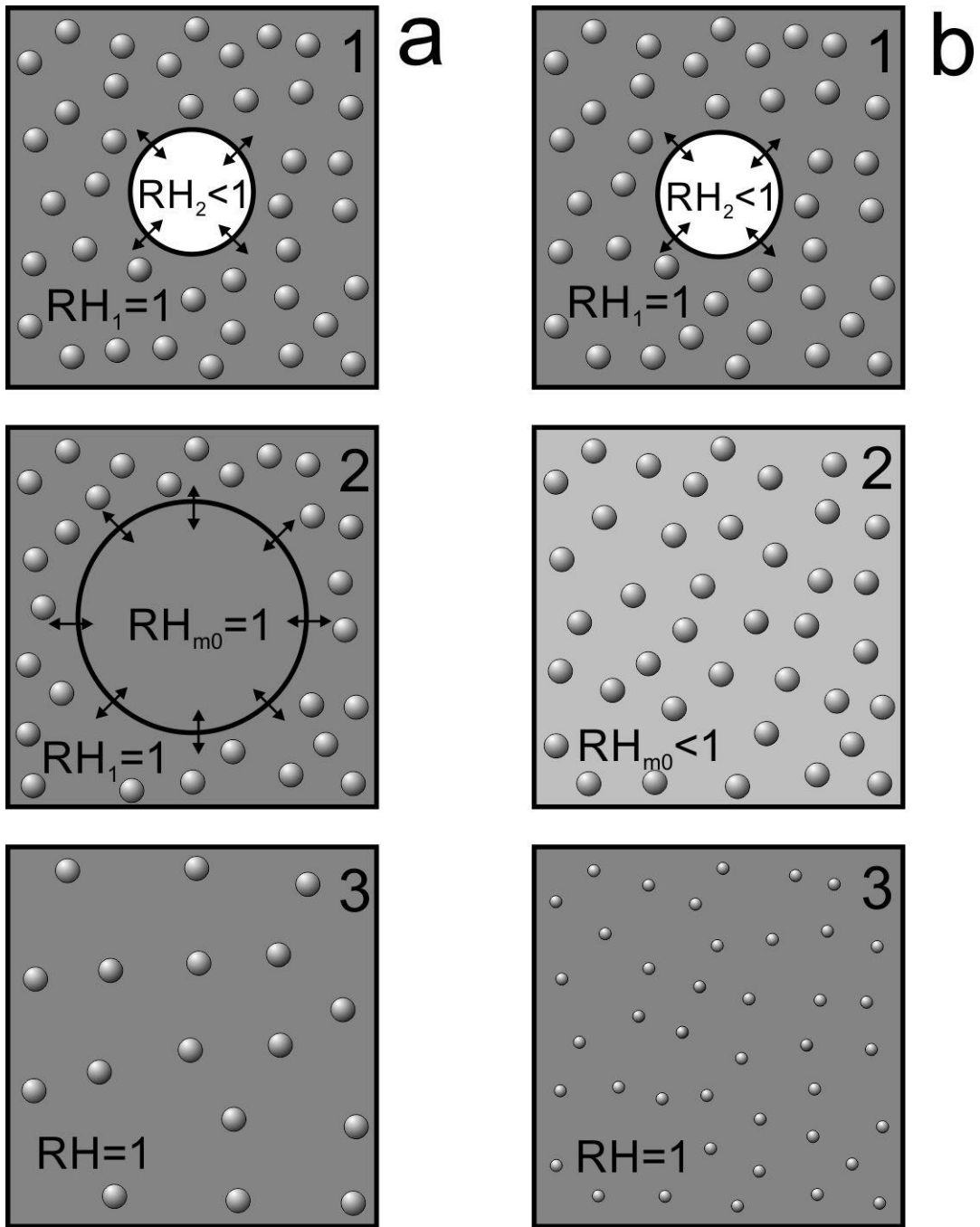
888 **Figure 13.** Spatial changes of particle concentration (a), extinction coefficient (b), liquid water  
889 content (c) and average and mean mass diameter (d) during transit through one of the  
890 convective clouds measured by CDP. The measurements were conducted during the  
891 COPE-MED project on 18 July, 2015. The sampling rate 10Hz ( $\sim 10\text{m}$  spatial resolution).  
892  $H=5500\text{m}$ ,  $T=-12\text{C}$ ,  $RH=0.2$ .

893 **Figure 14.** Relationships between (a)  $LWC(N)$ ; (b)  $\beta(N)$ ; (c)  $D_v(N)$ ; (d)  $LWC(\beta)$  calculated from  
894 the CDP measurements obtained during sampling several convective clouds. The  
895 measurements were conducted during the COPE-MED project on 18 July, 2015,  
896  $H=5500\text{m}$ ,  $T=-12\text{C}$ ,  $RH=0.2$ . The measurements were sampled at 10Hz ( $\sim 10\text{m}$  spatial  
897 resolution). Dashed lines are linear regressions. Red lines indicate primary  
898 inhomogeneous mixing dependencies calculated for the same environmental conditions.

899 **Figure 15.** Relationships between (a)  $LWC(N)$ ; (b)  $\beta(N)$ ; (c)  $D_v(N)$ ; (d)  $LWC(\beta)$  calculated from  
900 the CDP measurements sampled during traverse through 45 convective clouds. The  
901 measurements were conducted during the COPE-MED project on 02 August, 2015.  
902 Dashed lines indicate (a), (b) and (d) indicate the sectors, where the majority of the points  
903 are scattered. The altitude of sampling varied in the range  $3000\text{m} < H < 4500\text{m}$ ,  
904 temperature  $-11\text{C} < T < 0\text{C}$ , relative humidity in the vicinity of clouds  $15\% < RH < 65\%$ . The  
905 measurements were sampled at 10Hz ( $\sim 10\text{m}$  spatial resolution).

906 **Figure A1.** Amount of evaporated liquid water  $\delta q_m$  required for saturation of a cloud volume with  
907 initial humidity  $RH_m$ . Comparisons of the modeled  $\delta q_m$  and that calculated from Eqs.  
908 (A8) and (A9) for three temperatures  $T_{m0} = -20\text{C}$ ,  $0\text{C}$  and  $20\text{C}$ . Calculations were  
909 performed for  $P=880\text{mb}$ .

910



911

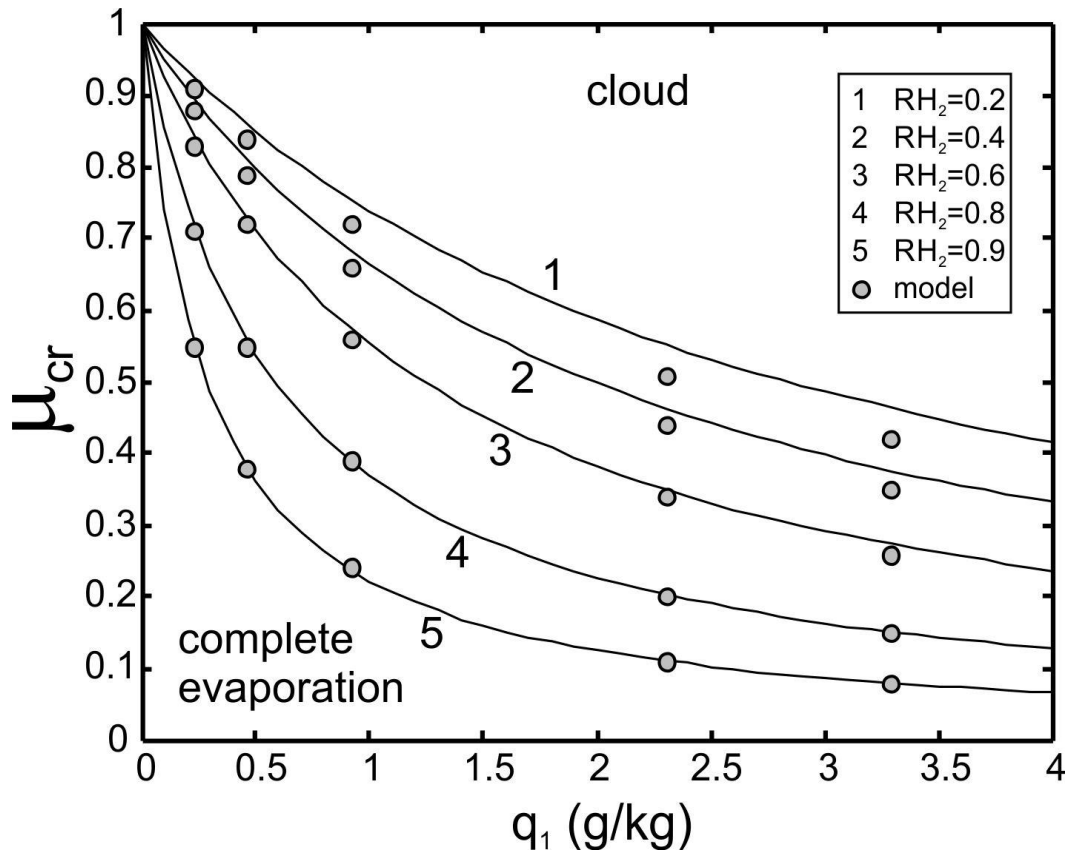
912

913 **Figure 1.** Classical conceptual diagram of (a) inhomogeneous and (b) homogeneous mixing. 1 initial state;

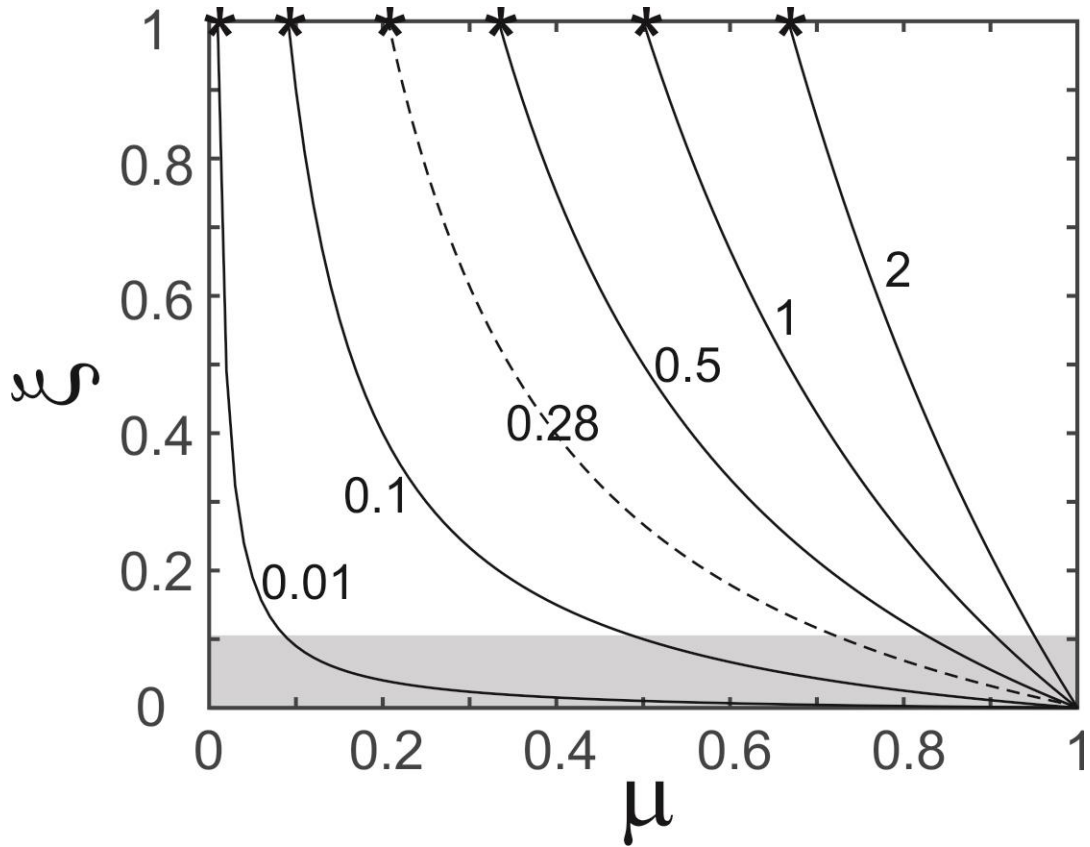
914 2 mixing state; 3 final state.

915

916

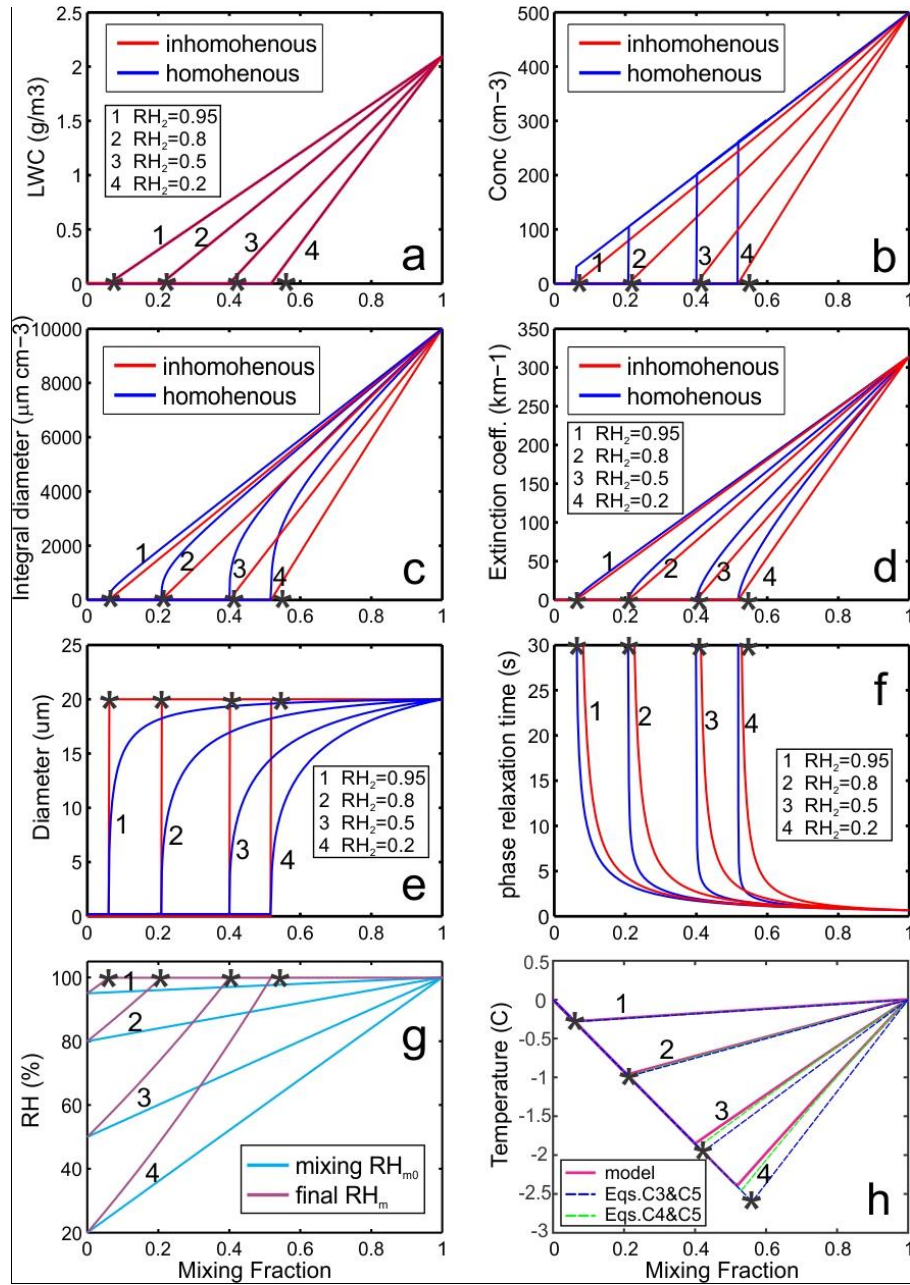


1  
2 **Figure 2.** Dependence of critical mixing fraction  $\mu_{cr}$  versus mixing ratio  $q_0$  calculated from Eq.(7). Circles  
3 indicate modeled points. The calculations were performed for  $T=0C$  and  $H=3000m$ .  
4



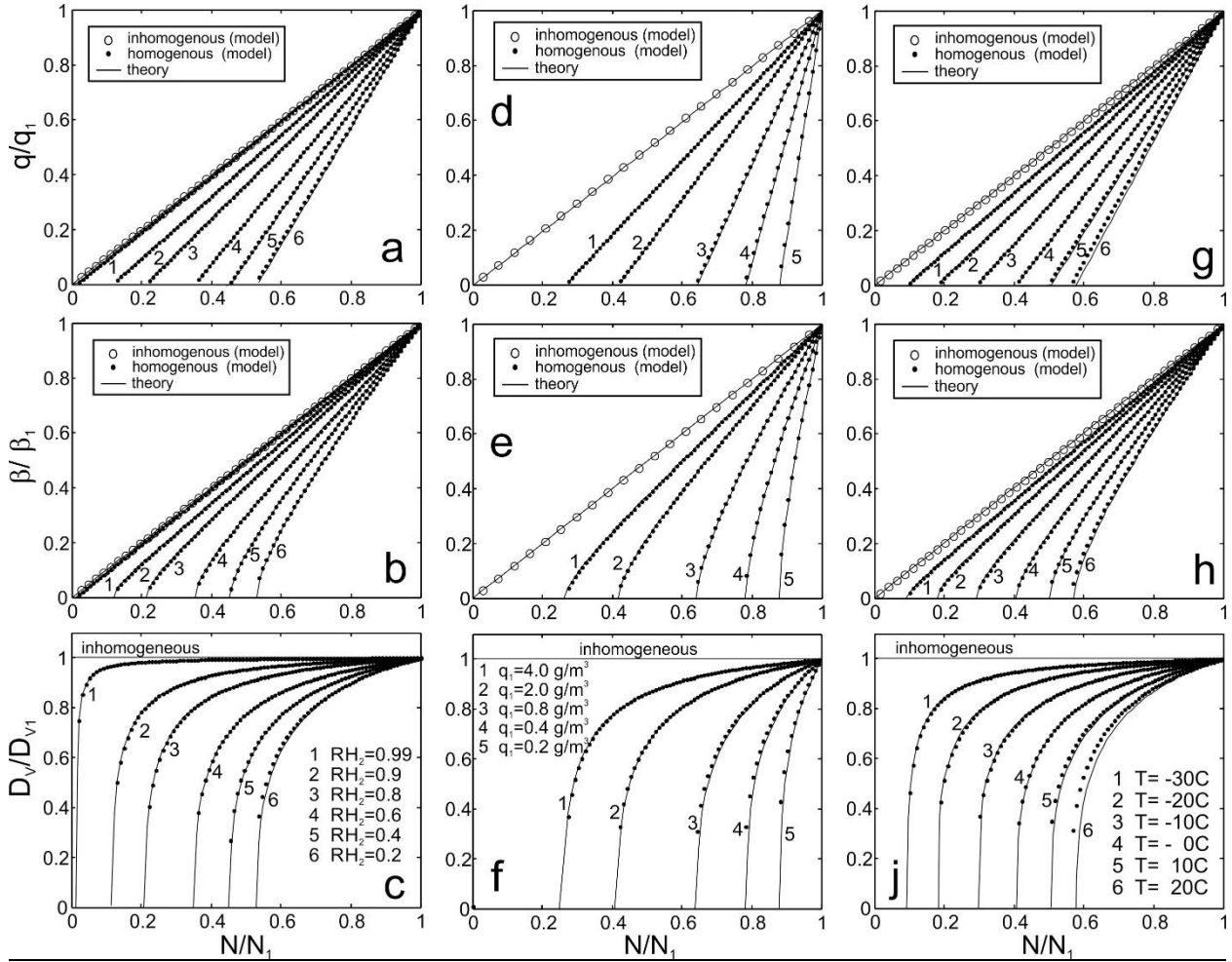
1  
2  
3  
4  
5  
6  
7

**Figure 3.** Dependence of  $\xi$  versus  $\mu$ . Numbers are the dimensionless ratios  $\delta q^*/q_1$ . Critical mixing ratios  $\mu_{cr}$  are indicated by stars. Grey area indicates area where the moments of homogeneous and extreme inhomogeneous mixing may not be segregated from in-situ measurements. Dashed line was calculated for the cloud in Figs.13-14.



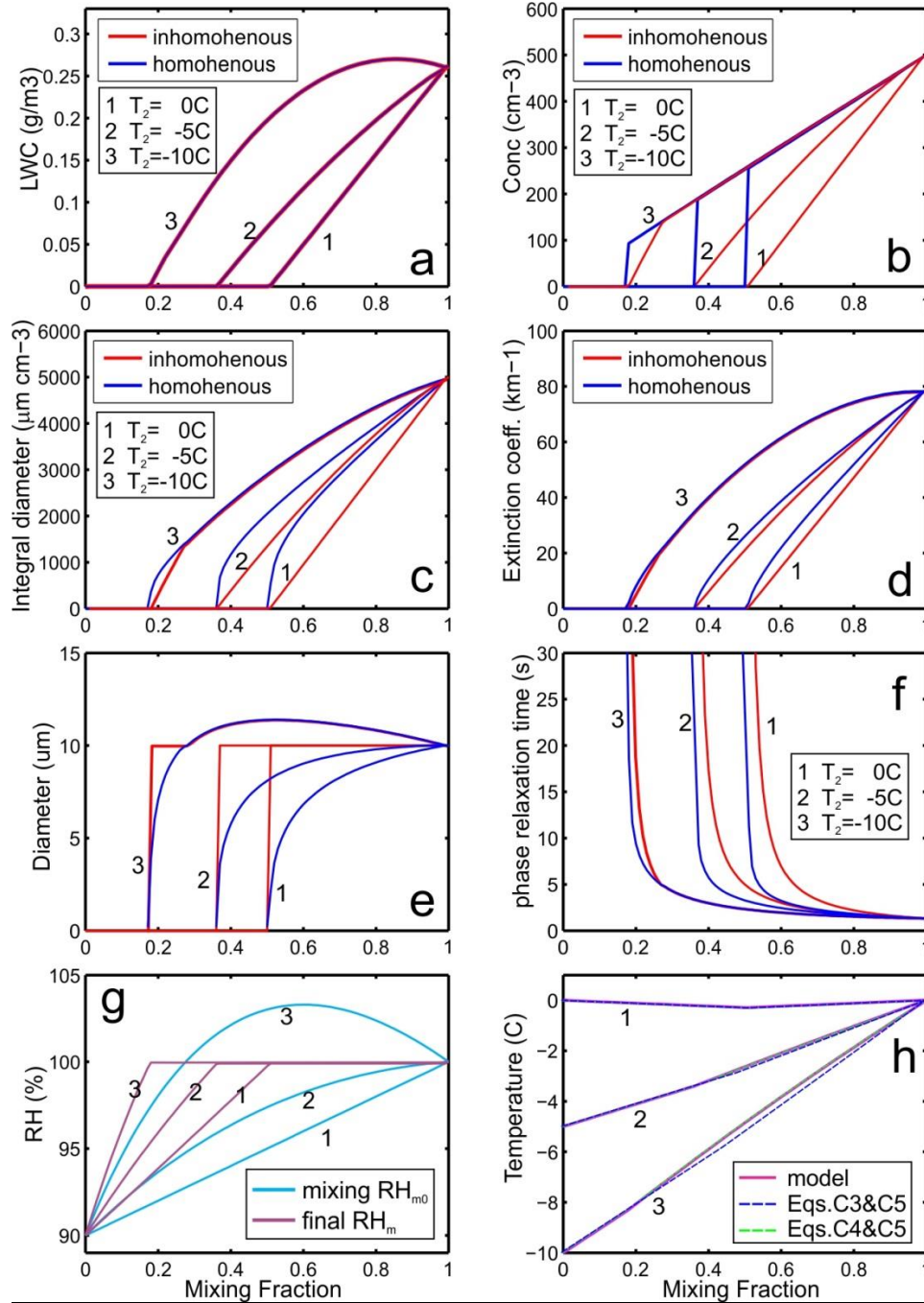
1  
2

3 **Figure 4.** Simulation of (a) liquid water mixing ratio, (b) droplet number concentration, (c) integral droplet  
4 diameter, (d) extinction coefficient, (e) mean volume diameter, (f) time of phase relaxation, (g) relative  
5 humidity in the mixed volume before droplet evaporation  $RH_{m0}$  and at the equilibrium state  $RH_m$ , (h) final  
6 temperature  $T_{m0}$  versus ratio of mixing  $\mu$  formed after homogeneous and extreme inhomogeneous mixing  
7 between dry and cloudy parcel with monodisperse droplets. Black stars indicate critical mixing fraction  
8  $\mu_{cr}$  calculated from Eq.(7). The calculations were performed for  $RH_2 = 0.2, 0.5, 0.8, 0.95$ ;  $D_1=20\mu\text{m}$ ,  
9  $N_1=500\text{cm}^{-3}$ ;  $T_1 = T_2 = 0\text{C}$ ;  $H=1000\text{m}$ .



1  
2  
3 **Figure 5.** Dependence of normalized liquid water mixing ratio  $q/q_1$  (a,d,g), extinction coefficient  $\beta/\beta_1$   
4 (b,e,h) and mean volume diameter  $D_v/D_{v1}$  (c,f,j) versus normalized number concentration  $N/N_1$  for  
5 various humidity of the entrained air (a,b,c), for various liquid water mixing ratios (d,e,f) and for various  
6 temperatures (g,h,j). The calculations were performed the initial conditions:  $H=1000\text{m}$ ,  $D_1=20\mu\text{m}$ ; for (a-  
7 c; g-j)  $N_1=500\text{cm}^{-3}$ ; for (a-f)  $T_1 = T_2 = 0\text{C}$ .

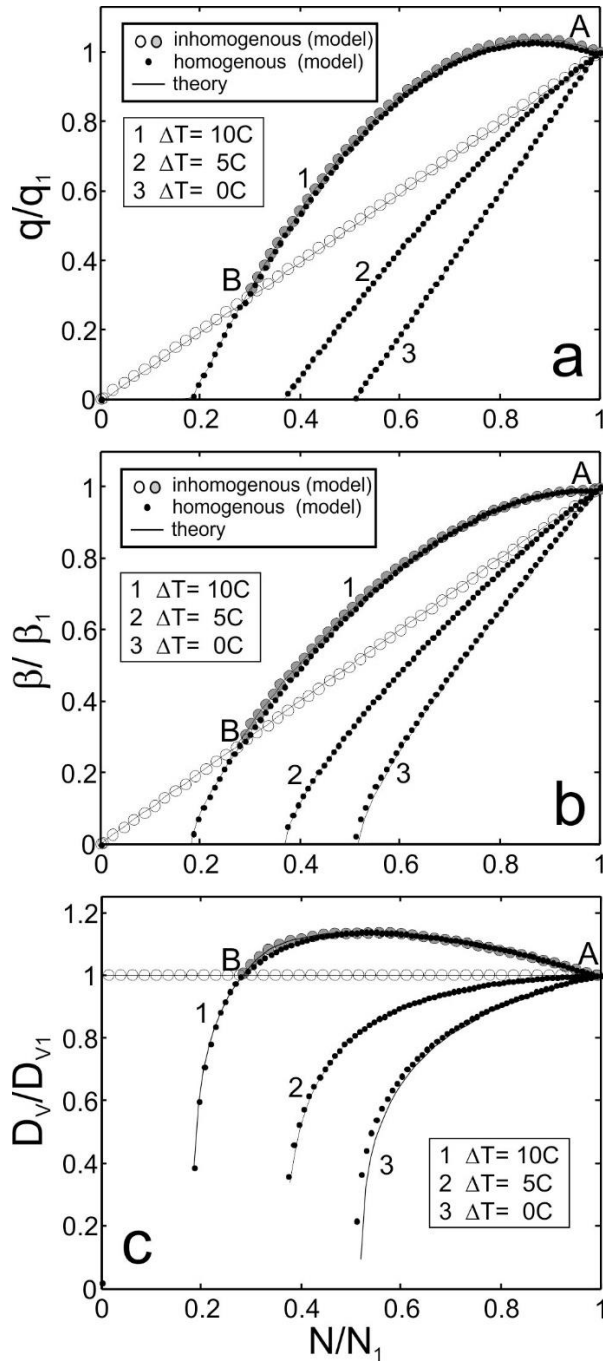
8



1  
2

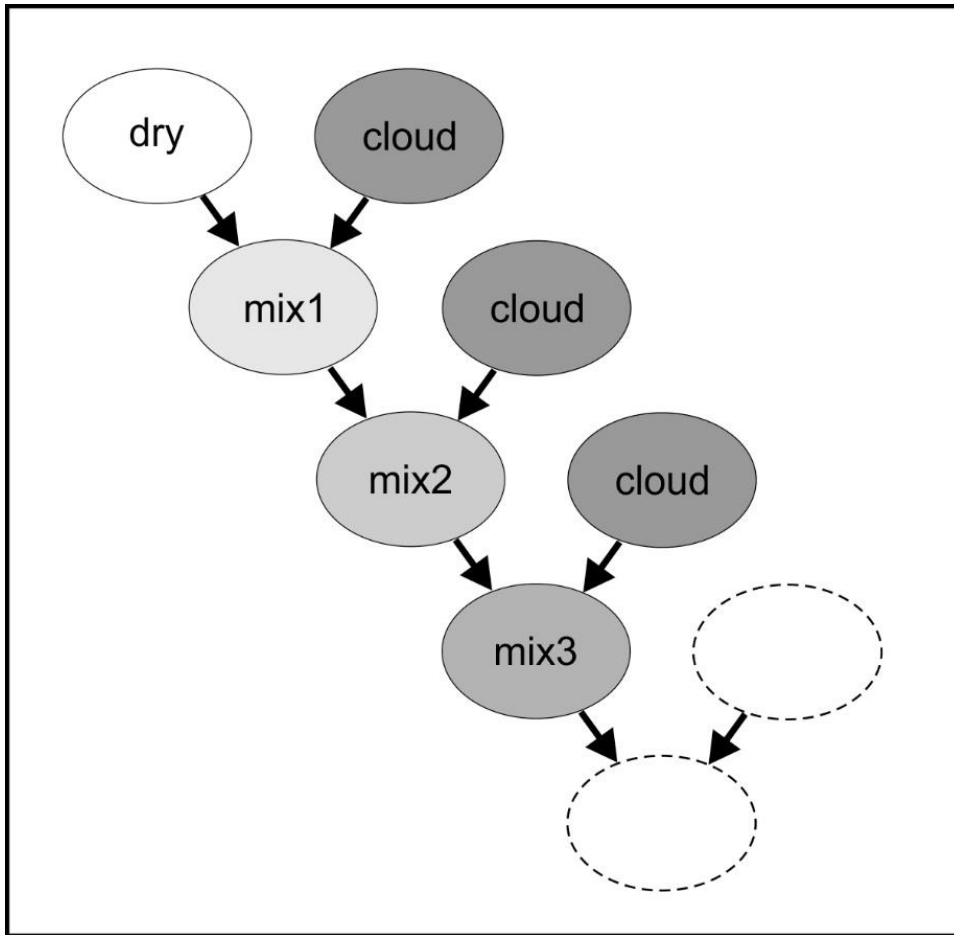
3 **Figure 6.** Simulation of (a) droplet number concentration and (b) liquid water mixing ratio, (c) integral  
4 droplet diameter, (d) extinction coefficient, (e) mean volume diameter, (f) time of phase relaxation, (g)  
5 relative humidity in the mixed volume before droplet evaporation  $RH_{m0}$  and at the equilibrium state  $RH_m$ ,  
6 (h) final temperature  $T_m$  versus ratio of mixing  $\mu$  formed after homogeneous and extreme inhomogeneous  
7 mixing between dry and cloudy parcel with monodisperse droplets. The calculations were performed for  
8  $RH_2=0.9$ ;  $D_1=10\mu\text{m}$ ,  $N_1=500\text{cm}^{-3}$ ;  $T_1 =0\text{C}$ ;  $T_2 = -10\text{C}, -5\text{C}, 0\text{C}$ ;  $H=1000\text{m}$ .





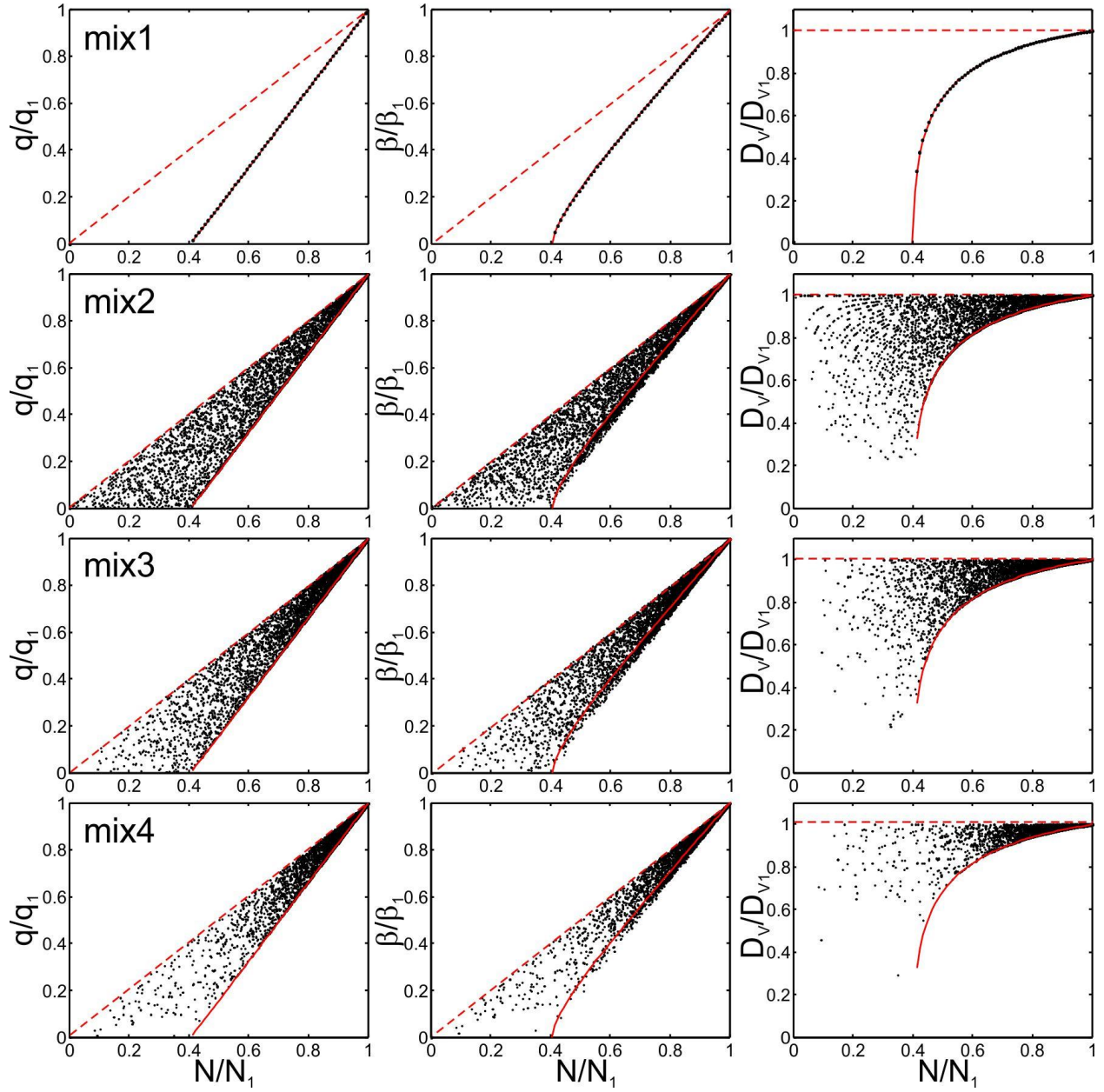
1  
2

3 **Figure 7.** Effect of temperature difference between cloud and entrained air on mixing. The calculations were  
 4 performed for initial temperatures  $T_2$ : (1) -10C; (2) -5C; (3) 0C. Grey circles indicate extremely  
 5 inhomogeneous mixing on line 1 at the AB interval. The rest cases on extremely inhomogeneous mixing are  
 6 indicated by open circles. The initial conditions used for the calculations were:  $H=1000\text{m}$ ,  $RH_2=90\%$ ;  
 7  $D_1 = 10\mu\text{m}$ ,  $N_1 = 500\text{cm}^{-3}$ ,  $T_1=0\text{C}$ .



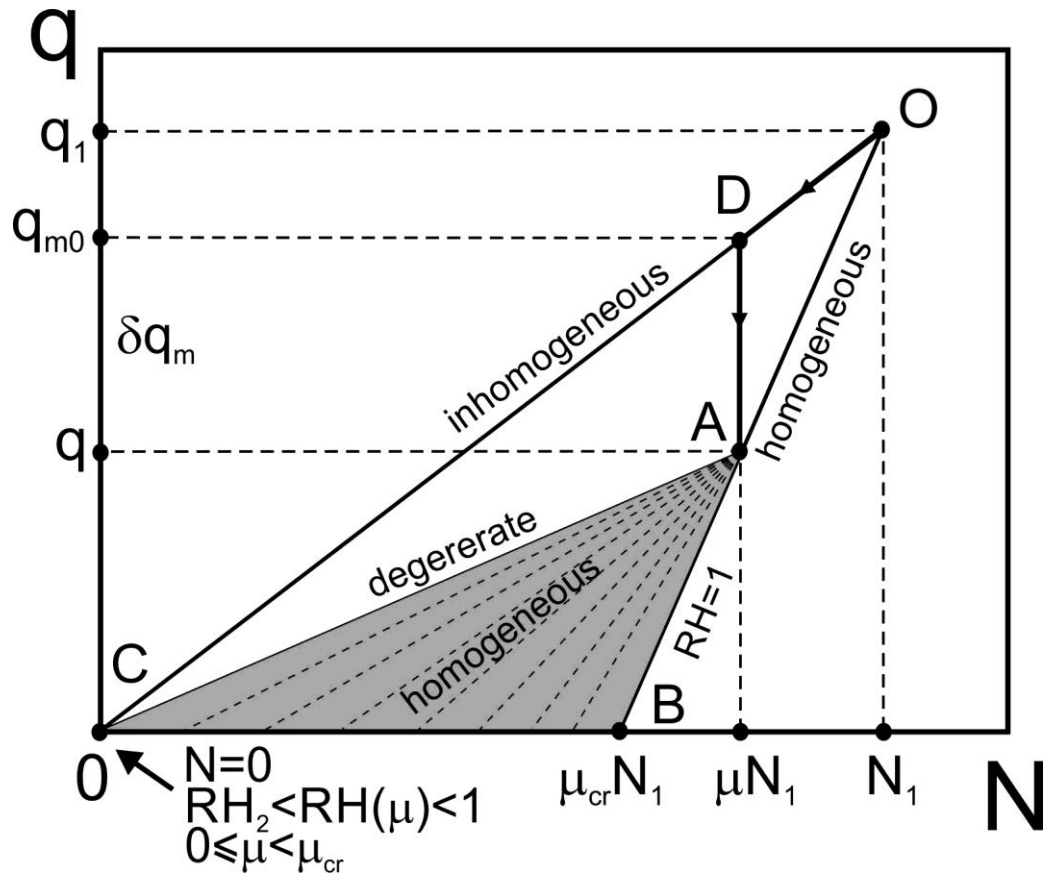
1  
2  
3  
4  
5  
6

**Figure 8.** Conceptual diagram of cascade mixing of the out-of-cloud entrained parcel with the cloudy environment



7  
8  
9  
10  
11  
12

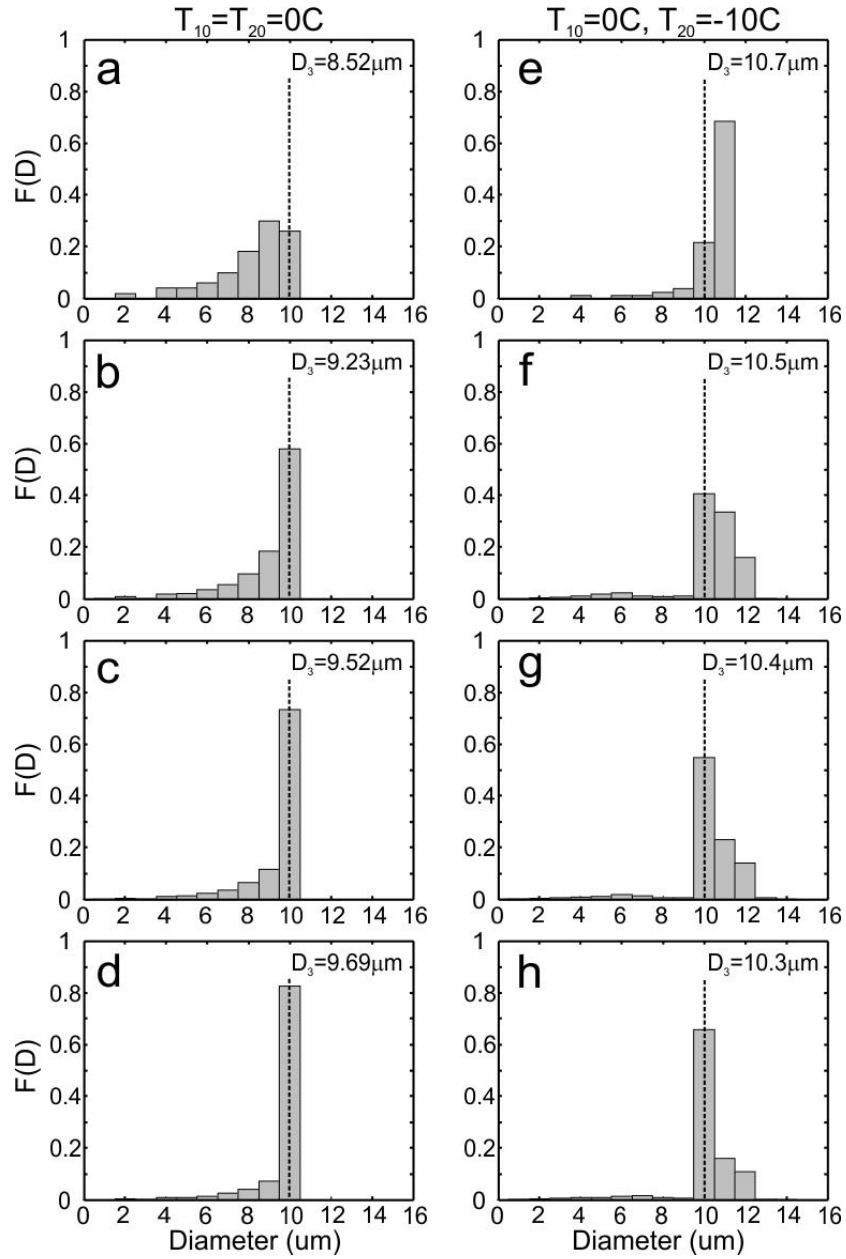
**Figure 9.** Simulation of stochastic mixing corresponding to stages 1-4 as indicated in Fig.8. Solid red lines indicate the normalized dependences  $q$ ,  $\beta$ ,  $D_v$  vs.  $N$  for the primary stage of homogeneous mixing. Dashed red lines indicate the same dependences for inhomogeneous mixing. The initial conditions used for the simulations were:  $H=1000\text{m}$ ,  $T_1 = T_2 = 0\text{C}$ ;  $RH_2=0.5$ ;  $D_1 = 10\mu\text{m}$ ,  $N_1 = 500\text{cm}^{-3}$ .



1  
2  
3  
4  
5

**Figure 10.** Conceptual diagram explaining breaking the functional relationships between the microphysical moment during progressive missing (see text).

1



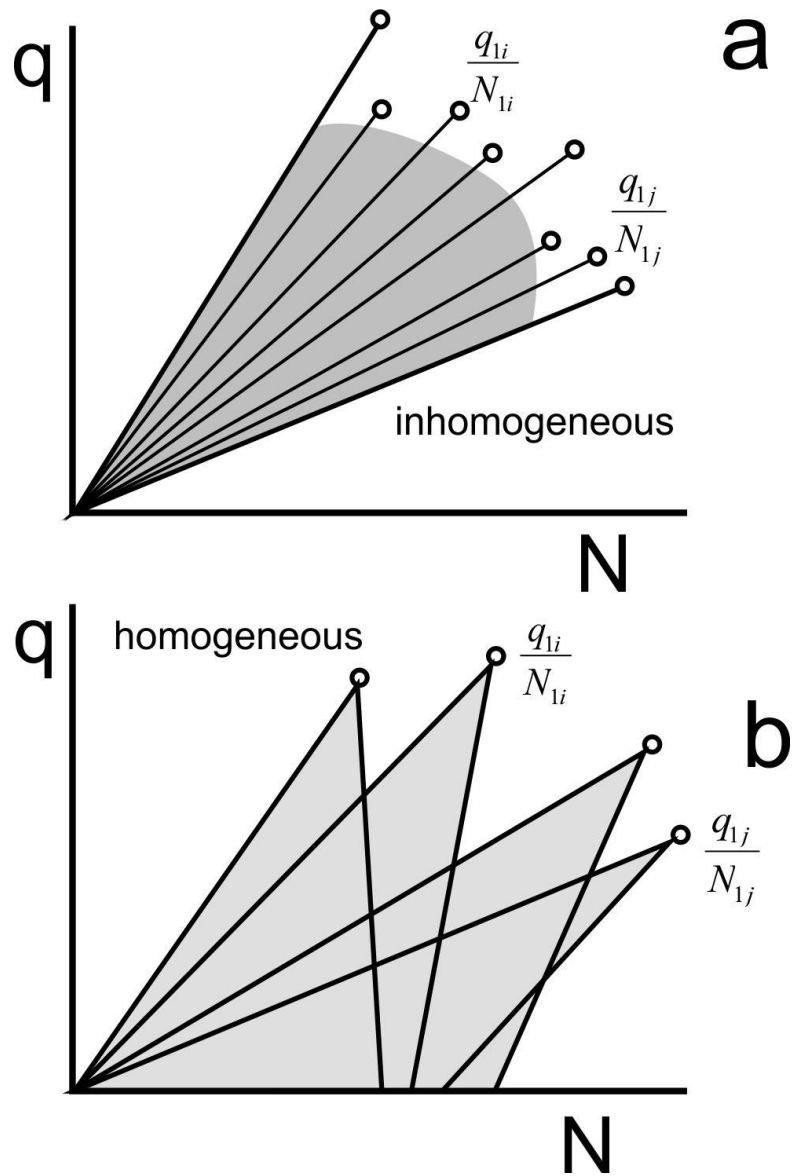
2

3

4 **Figure 11.** Droplet size distributions formed during the progressive homogeneous mixing corresponding  
 5 to the (a,e) primary stage; (b,f) 2<sup>nd</sup> stage; (c,g) 3<sup>rd</sup> stage; (d,h) 4<sup>th</sup> stage. Left column (a,b,c,d) corresponds  
 6 to the case, when the cloud temperature is equal to the dry air temperature  $T_1 = T_2 = 0^\circ\text{C}$ .; right column  
 7 (e,f,g,h) corresponds to the case when  $T_1 = 0^\circ\text{C}$ ,  $T_2 = -10^\circ\text{C}$ . For both cases the simulation was performed  
 8 for  $D_1 = 10\mu\text{m}$ ;  $N = 500\text{cm}^{-3}$ ;  $RH_2 = 0.9$ .

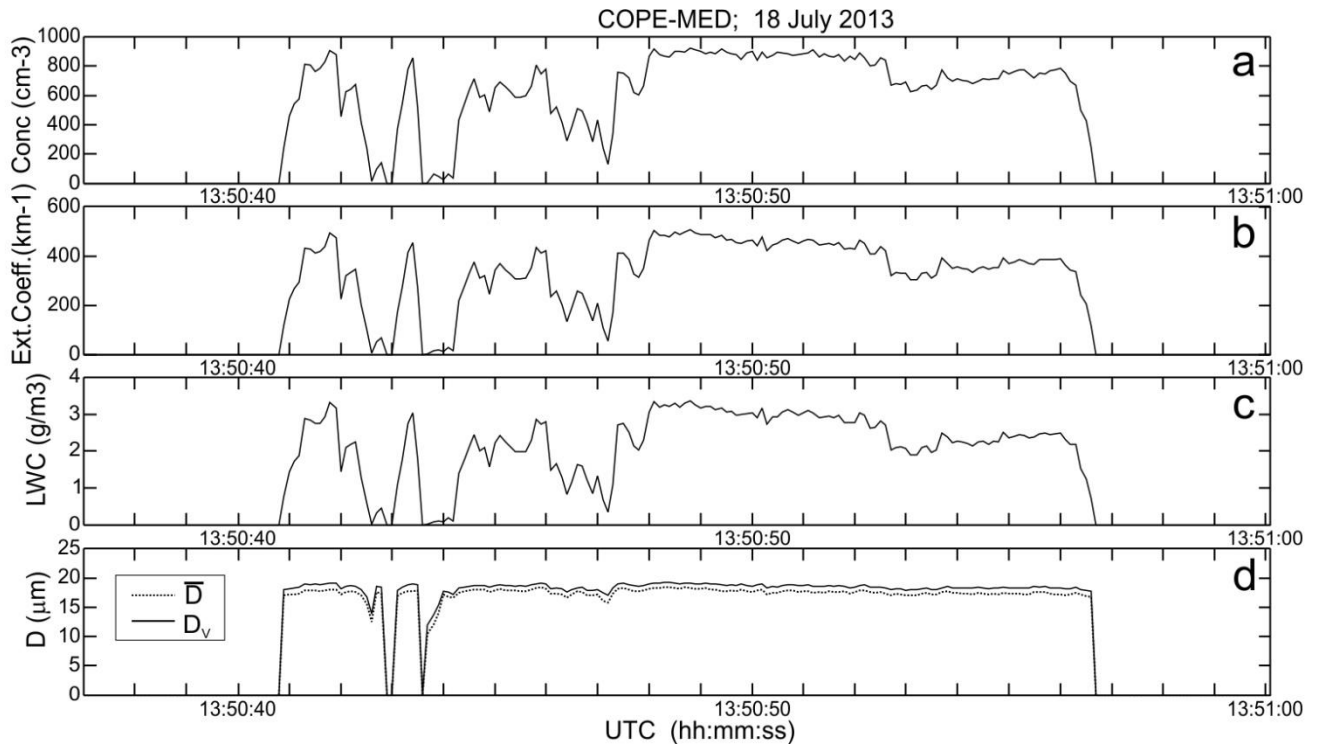
9

1  
2



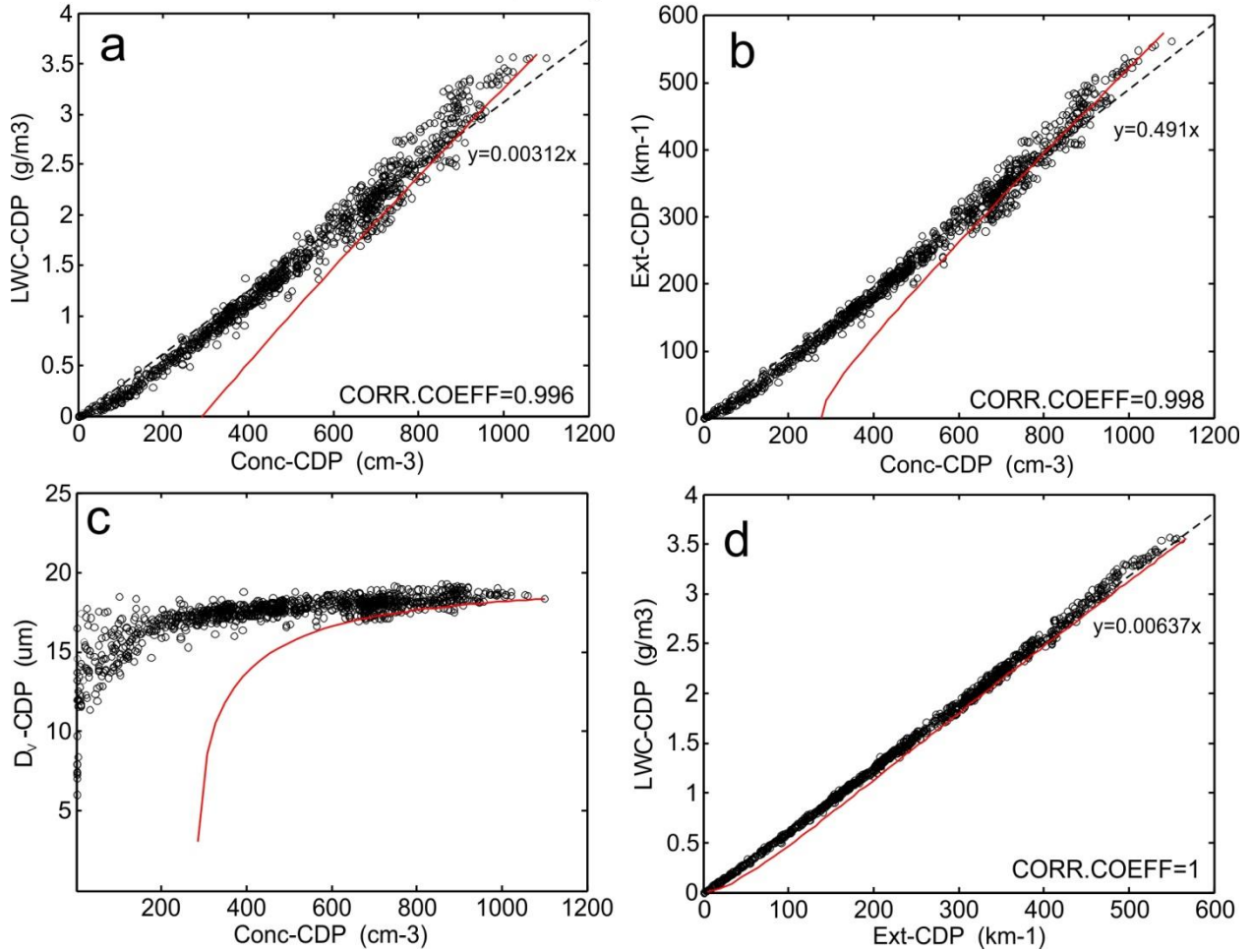
3  
4  
5  
6  
7  
8

**Figure 12.** Conceptual diagrams of scattering of measurements of  $q$  versus  $N$  for (a) extreme inhomogeneous and (b) homogeneous mixing.



1  
2  
3  
4  
5  
6

**Figure 13.** Spatial changes of particle concentration (a), extinction coefficient (b), liquid water content (c) and average and mean mass diameter (d) during transit through one of the convective clouds measured by CDP. The measurements were conducted during the COPE-MED project on 18 July, 2015. The sampling rate 10Hz (~10m spatial resolution).  $H=5500\text{m}$ ,  $T=-12\text{C}$ ,  $RH=0.2$ .

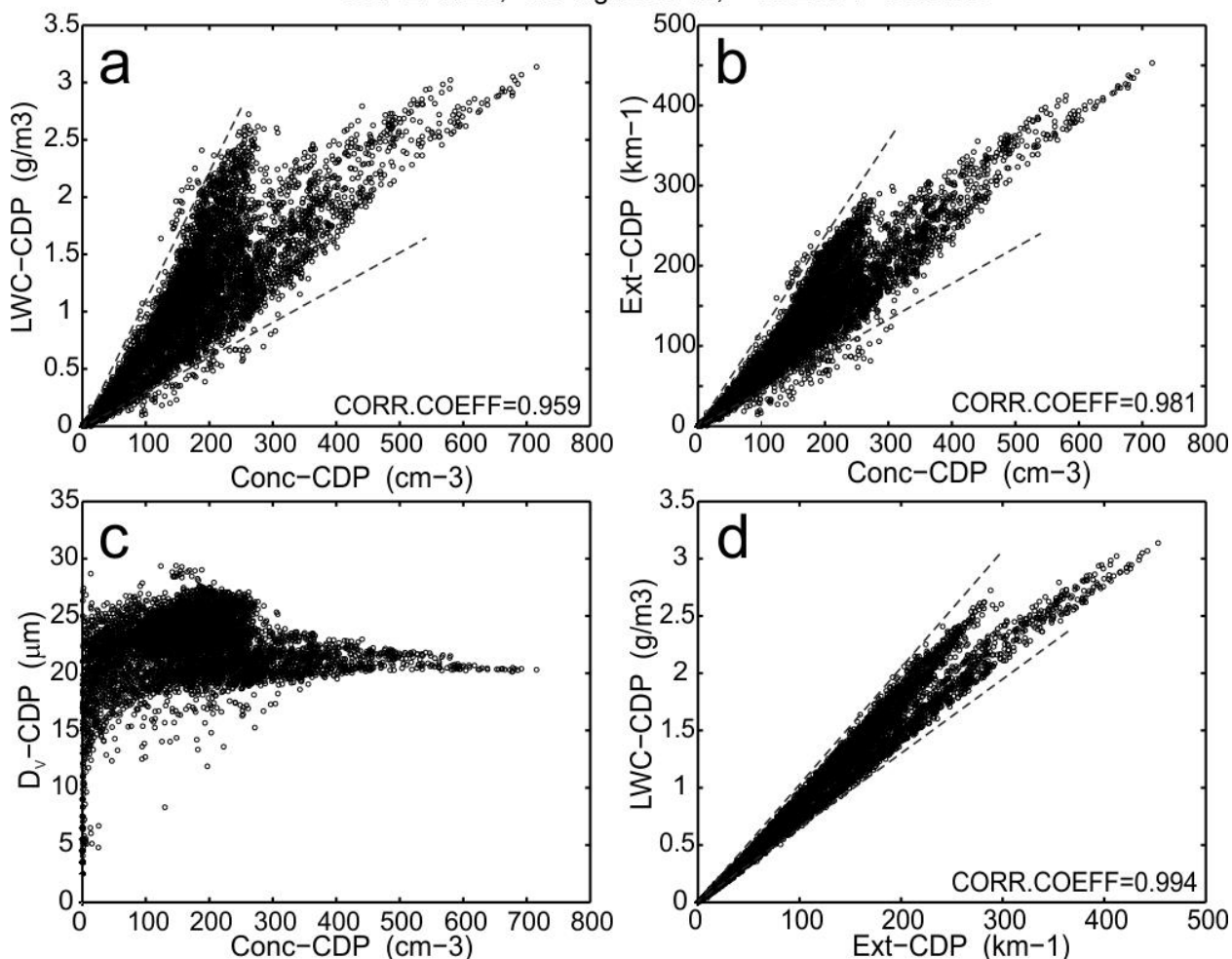


1  
2  
3  
4  
5  
6  
7  
8  
9  
10

**Figure 14.** Relationships between (a)  $LWC(N)$ ; (b)  $\beta(N)$ ; (c)  $D_v(N)$ ; (d)  $LWC(\beta)$  calculated from the CDP measurements obtained during sampling several convective clouds. The measurements were conducted during the COPE-MED project on 18 July, 2015,  $H=5500\text{m}$ ,  $T=-12\text{C}$ ,  $RH=0.2$ . The measurements were sampled at 10Hz ( $\sim 10\text{m}$  spatial resolution). Dashed lines are linear regressions. Red lines indicate primary inhomogeneous mixing dependencies calculated for the same environmental conditions.



COPE-MED; 02 August 2013; 13:25:01-15:38:06



1  
2  
3  
4  
5  
6  
7  
8  
9  
10

**Figure 15.** Relationships between (a)  $LWC(N)$ ; (b)  $\beta(N)$ ; (c)  $D_v(N)$ ; (d)  $LWC(\beta)$  calculated from the CDP measurements sampled during traverse through 45 convective clouds. The measurements were conducted during the COPE-MED project on 02 August, 2015. Dashed lines indicate the sectors, where the majority of the points are scattered. The altitude of sampling varied in the range  $3000m < H < 4500m$ , temperature  $-11C < T < 0C$ , relative humidity in the vicinity of clouds  $15% < RH < 65%$ . The measurements were sampled at 10Hz ( $\sim 10m$  spatial resolution).

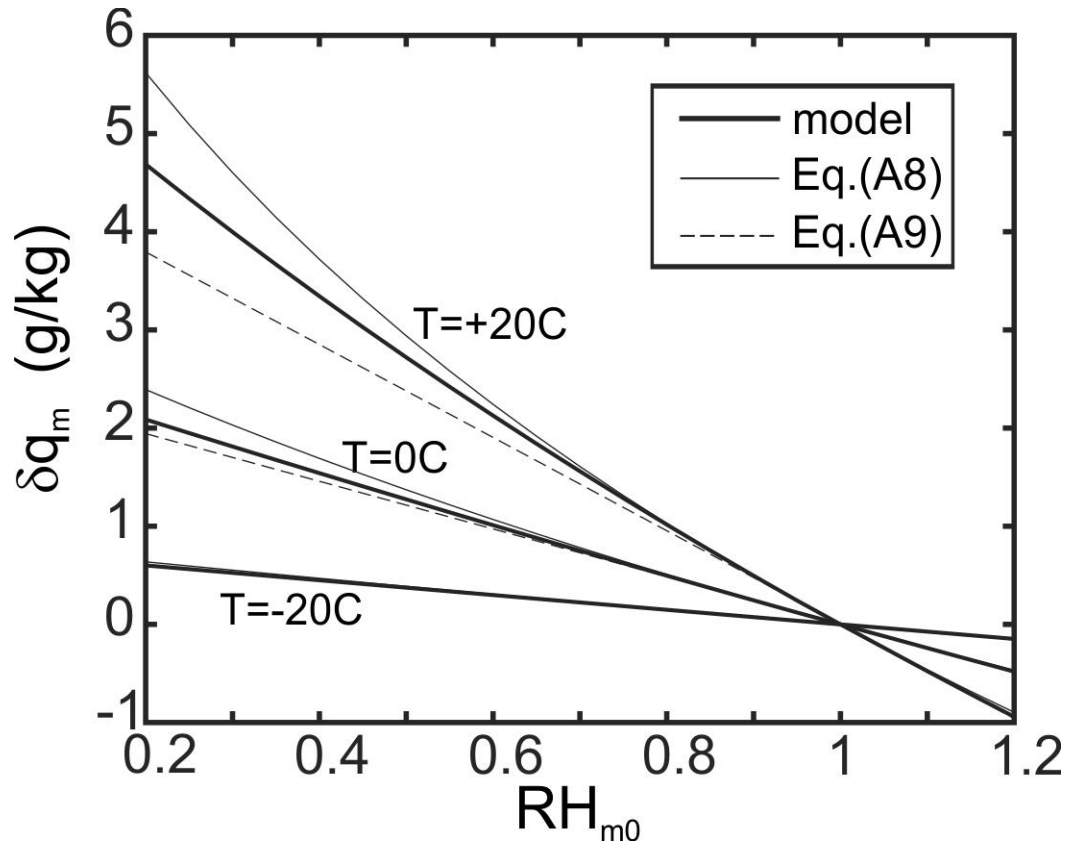


**Figure A1.** Amount of evaporated liquid water  $\delta q_m$  required for saturation of a cloud volume with initial humidity  $RH_m$ . Comparisons of the modeled  $\delta q_m$  and that calculated from Eqs. (A8) and (A9) for three temperatures  $T_{m0} = -20\text{C}$ ,  $0\text{C}$  and  $20\text{C}$ . Calculations were performed for  $P=880\text{mb}$ .